

AN ABSTRACT OF THE THESIS OF

Kevin Konrad for the degree of Master of Science in Geology presented on October 5, 2012

Title: Helium Isotope Variations in Peridotite, Gabbro and Basalt from the Kane Oceanic Core Complex

Abstract approved:

David W. Graham

The Kane Oceanic Core Complex (OCC) is a valuable window into crustal architecture and chemical composition of the lithosphere beneath a slow-spreading ocean ridge. A suite of > 30 samples (comprised of whole rocks, mineral separates and basalt glasses) has been analyzed for $^3\text{He}/^4\text{He}$ isotope ratios and He concentrations. Gas extraction experiments included crushing in vacuum, step heating and fusion in a high-vacuum furnace. We found $^3\text{He}/^4\text{He}$ in the two freshest peridotites (harzburgite and olivine websterite) to be identical to ratios measured in basalt glasses collected from the Kane fracture zone-ridge axis intersection (8.4–8.7 R_A). Notably, the freshest and least deformed peridotite (a porphyroclastic harzburgite) has the highest helium content of any of the OCC ultramafic rocks (170 ncc STP/g), while the majority of its helium (70%) is released only upon melting. Lower helium contents (1–45 ncc STP/g) and more variable

$^3\text{He}/^4\text{He}$ (2.0-6.3 R_A) are found in other more altered/deformed peridotite samples (whole rocks, clinopyroxene and orthopyroxene separates). For example, three mylonitized peridotites have lower helium contents compared to the less deformed peridotites. Troctolite intrusions from the Adam and Eve Domes appear to record very late-stage melt impregnation fed through dunite conduits near the MOHO. $^3\text{He}/^4\text{He}$ in these troctolites overlaps with values in the fresh peridotites and axial basalts, but extends to slightly higher values (8.6-9.0 R_A). Collectively, fresh Kane peridotites and troctolites having He concentrations above 10 ncc STP/g show $^3\text{He}/^4\text{He}$ ratios of 8.4-9.0 R_A that are higher than the median value (8.0-8.2 R_A) for mid-ocean ridge basalts. This suggests that domains of depleted upper mantle in the Kane region tend to have $^3\text{He}/^4\text{He}$ ratios of 9 R_A or higher, similar to what is observed in the most trace-element depleted MORBs globally. Kane gabbroic rocks are more variable in $^3\text{He}/^4\text{He}$. A subset of gabbros show systematically lower $^3\text{He}/^4\text{He}$ ratios (0.9-7.2 R_A), with He concentrations of 1-24 ncc STP/g, reflecting the increased importance of atmospheric and radiogenic components in several cases. Nonetheless, two whole rock gabbroic samples plus an amphibole separate have $^3\text{He}/^4\text{He}$ ratios of 7.6-8.0 R_A and He contents between 13 and 57 ncc STP/g. Variation in the sampling of a lithologically heterogeneous mantle source by the partial melting process may account for the observed $^3\text{He}/^4\text{He}$ variability of 7.6-9.0 R_A in peridotite, gabbro and basalt in the Kane area.

©Copyright by Kevin Konrad

October 5, 2012

All Rights Reserved

Helium Isotope Variations in Peridotite, Gabbro and Basalt from the Kane Oceanic Core

Complex

by

Kevin Konrad

A THESIS

Submitted to

Oregon State University

In partial fulfillment of

the requirements for the

degree of

Master of Science

Presented October 5, 2012

Commencement: June 2013

Master of Science thesis of Kevin Konrad presented on October 5, 2012.

APPROVED:

Major Professor, representing Geology and Geophysics

Dean of the College of Earth, Ocean, and Atmospheric Sciences

Dean of the Graduate School

I understand that my thesis will become part of the permanent collection of Oregon State University libraries. My signature below authorizes release of my thesis to any reader upon request.

Kevin Konrad, Author

ACKNOWLEDGEMENTS

There are many people I would like to thank for helping me get here today. I would like to thank David Graham for taking me as a graduate student and dealing with me for these last two years. Your blunt honesty is refreshing and always welcomed. I would like to express sincere gratitude to the members of my committee. I would like to thank Adam Kent for all his assistance with analyzing trace elements and discussing the data. Conversations about petrology and crustal accretion with Roger Nielsen were invaluable to the discussion of this project.

I am grateful to Dr. Henry Dick for providing the rocks used in this project along with maps and information on the Kane OCC. Margaret Sulanovska provided glasses used in this study from the Woods Hole repository.

I would like to thank my family for helping me get to where I am today. Most of all I would like to thank my wife Andrea Balbas. Without her constant moral support I would still be sitting in a basement in Queens, NY (not a good thing). I can't imagine a life without our scientific debates, adventures in the field, cats, and lovely home. Let this thesis be the definitive proof that I love her more.

TABLE OF CONTENTS

	<u>Page</u>
1.0 Introduction-----	1
1.1 Isotopic variability between peridotite and MORB-----	1
1.2 Geologic Setting: Kane area Mid-Atlantic Ridge-----	4
2.0 Questions Addressed-----	7
3.0 Sampling and Methods -----	8
3.1 Rock Sampling -----	8
3.2 Helium isotope analysis-----	11
3.3 Microprobe and laser ablation analyses -----	19
4.0 Results -----	21
4.1 Basalts-----	22
4.2 Ultra-mafics-----	23
4.3 Primitive gabbros (troctolites and troctolitic gabbro) -----	25
4.4 Gabbro-----	29
4.5 Evolved gabbro-----	30
4.6 Carbon dioxide from crushed peridotite and gabbro samples-----	34
5.0 Discussion-----	34
5.1 Helium isotopic structure of the oceanic lithosphere at the Kane OCC-----	35
5.1.1 Adam dome-----	35
5.1.2 Cain and Abel Domes-----	37
5.2 Melting history beneath the Kane OCC-----	38
5.3 Melt-wallrock interaction and the representative nature of peridotite, gabbro and basalt-----	42
5.4 Role of shearing, alteration and metamorphism of peridotite-----	43
5.5 Analyzing ocean lithospheric rocks-----	45
5.5.1 Crushing-----	45
5.5.2 Melting analysis-----	47
6.0 Summary-----	48
7.0 References-----	50
Appendix-----	54

LIST OF FIGURES

<u>Figure</u>	<u>Page</u>
1 Bathymetric map of the Kane Oceanic Core Complex showing sample localities for this study -----	6
2 $^3\text{He}/^4\text{He}$ plotted versus total ^4He concentration for the entire sample suite--	21
3 $^3\text{He}/^4\text{He}$ plotted versus $1/^4\text{He}$ concentration illustrating the effects of sample alteration-----	27
4 Rare earth element patterns for selected samples-----	31
5 $^3\text{He}/^4\text{He}$ versus CO_2 concentration for lithospheric rocks-----	32
6 Schematic representation of two stages in the melting history beneath the Kane area-----	39
7 Deformation grade versus $[\text{He}]$ and $^3\text{He}/^4\text{He}$ ratio measured from the total melted extraction -----	42
8 $^3\text{He}/^4\text{He}$ versus ^4He concentration of crushed analyses of samples run with and without baking.-----	44

LIST OF TABLES

<u>Table</u>		<u>Page</u>
1	Sample lithology and location-----	9
2	Helium Isotope and He and CO ₂ concentrations for Rocks from the Kane OCC and Adjacent Ridge Axis-----	14
3	Select major and trace element data-----	20

1. INTRODUCTION

A fundamental assumption in mapping the chemical and isotopic variability of the upper mantle is that the isotope composition of mid-ocean ridge basalts (MORBs) is representative of the mantle source region, being largely unmodified during magma transport through the crust and eruption on the seafloor. We have begun to test this assumption through measurement of He isotopes in a suite of rocks from the Kane Oceanic Core Complex (OCC) along the Mid-Atlantic Ridge (23°N).

1.1 Isotopic variability between peridotite and MORB

To date, there are only a few noble gas isotope investigations of lower crustal and upper mantle rocks from ocean ridge settings. [Staudacher et al. \(1989\)](#) reported $^3\text{He}/^4\text{He} = 6.5 R_A$ (where R_A is the atmospheric ratio of 1.39×10^{-6}) for an incremental heating analysis of a hornblende peridotite from St. Paul's Rocks in the equatorial Atlantic Oceans. Both the $^3\text{He}/^4\text{He}$ and He concentration in this rock were similar to values reported for basalts from the same area ([Graham et al. 1992](#)). A study by [Kumagai et al. \(2003\)](#) of several gabbros and two peridotites from Atlantis Bank, an oceanic core complex in the Indian Ocean, showed some samples with $^3\text{He}/^4\text{He}$ ratios similar to the typical range in mid-ocean ridge basalts (6-9 R_A), indicating that plutonic and upper mantle rocks from ridge environments sometimes retain their primary $^3\text{He}/^4\text{He}$ signature. [Moreira et al. \(2003\)](#) found He isotope ratios in gabbroic rocks from Site 735B in the Indian Ocean as high as 8.6 R_A , and overlapping with the known range of MORBs (~6-10 R_A away from high ^3He hotspots). In contrast, atmospheric Ne isotope compositions were found to characterize those lower crustal rock types. [Kurz et al. \(2009\)](#) found most of the helium in Southwest Indian Ridge peridotites was released by melting compared to crushing, indicating

that their helium is mostly contained within mineral lattices rather than in fluid or melt inclusions. They also found increasing concentrations of helium with increasing degree of deformation in mylonitic peridotites, suggesting that mantle helium can be introduced into minerals during deformation/metamorphism at depth.

There are also only a couple studies where other isotope systems have been compared between peridotites and associated basalts, primarily from slow spreading ridge localities (*Salters and Dick 2002; Cipriani et al. 2004*). The Nd isotope compositions of peridotite and spatially associated basalt along the Southwest Indian Ridge show little overlap, which *Salters and Dick (2002)* interpret to result from preferential sampling of enriched mantle veins during magma genesis. In contrast, *Cipriani et al. (2004)* found that the mean $^{143}\text{Nd}/^{144}\text{Nd}$ for peridotite from the Vema Fracture Zone (representing 20 Myr of accretion along this portion of the Mid-Atlantic Ridge) was statistically indistinguishable from the local basalt. They did observe considerably more variability in the peridotites, however, and an inverse correlation between $^{143}\text{Nd}/^{144}\text{Nd}$ with spinel Cr#. The correlation was interpreted to indicate some control on the degree of melting by chemical heterogeneity in the peridotite, with the associated isotopic heterogeneity being preserved through the melting process. The feedback between mantle heterogeneity and partial melting is currently a topic of considerable interest in chemical geodynamics (e.g., *Katz and Weatherley 2012*). The compositional and isotopic variability in abyssal peridotite reflects the interplay of two processes: 1) fractional melting and melt extraction to the point at which clinopyroxene is nearly exhausted (e.g., *Johnson et al. 1990*), and 2) interaction with low pressure (< 5 kbar) partial melts (e.g., *Elthon 1992; Kelemen et al. 1997; Asimow 1999*). While volatile-rich melts with low viscosity and density become mobile at low mantle porosities (melt fractions ~0.01%), basaltic melts become mobile at porosities above 1%

(*Faul 2001*). Microtextures of abyssal peridotites from the Southwest Indian Ridge (SWIR) and Kane Fracture Zone reveal the presence of very small amounts of clinopyroxene, spinel and sulfide that crystallized from a trapped partial melt generated in the spinel stability field or shallower (*Seyler et al. 2001*). Metasomatic mineral inclusions (primarily diopside associated with minor apatite, amphibole, mica, albite and sulfide) trapped within orthopyroxene in some abyssal harzburgites appear to represent low degree partial melts of more fertile mantle, or melts of pyroxenite (*Seyler et al. 2004*). Because these peridotites have <2% modal clinopyroxene, they unlikely represent the residue of a single stage of melting beneath the SWIR given its deep axial ridge and ultra-low magma production. Such harzburgites must be residues of older melting events, and represent ancient refractory mantle, possibly trapped within the asthenosphere for the last 1-2 Gyr based on their ancient Re depletion ages (e.g., *Brandon et al. 2000; Alard et al. 2005; Harvey et al. 2006*). A recent seismic survey orthogonal to seafloor magnetic isochrons south of Bermuda (*Lizzaralde et al. 2004*) also provides geophysical evidence that melt retention in the shallow mantle can be significant. That survey revealed that the seismic velocity gradient in the upper 20-40 km of the mantle changed abruptly at a time when seafloor spreading rates decreased. These changes are correlated with changes in seafloor basement topography and crustal thickness. The observations may be explained by changes in the efficiency to which melt was extracted from beneath the ridge, with increased melt retention at slower spreading rate (*Lizzaralde et al. 2004*). When such processes operate, the range in isotope composition of incompatible elements, such as He, that is preserved in upper mantle rocks could well be larger than what is observed in basaltic melts erupted on the seafloor due to differences in the degree of homogenization during magma transport.

Here we present new helium isotope results for a comparative study of peridotite, gabbro and basalt along the Mid-Atlantic Ridge near the Kane transform. These results allow us to begin to test the linkages between mantle heterogeneity and the melting process beneath mid-ocean ridges from a noble gas viewpoint.

1.2 Geologic Setting: Kane Area Mid-Atlantic Ridge (MAR):

The Kane OCC provides an excellent window into the structure and composition of the oceanic crust along the MAR ([Dick et al. 2006, 2008](#)). It is located between 23°15'N and 23°45'N, and roughly 33 km west of the current MAR rift valley. The area covers ~ 20x35 km² of ~3 Ma oceanic floor ([Williams 2007](#)) and locally the seismic structure reveals a crustal thickness of ~5 km ([Morris and Detrick 1991](#)). Core complexes are believed to form by “run-away” faulting where little magmatic activity coupled with asymmetric spreading rates at ocean ridges produce long-lived detachment faults ([MacLeod et al. 2009](#)). This core complex exposes the entire suite of what is considered a ‘normal’ type lithosphere, which produces ‘normal’ MORBs (N-MORBs) ([Bryan et al. 1981; Dick et al. 2008](#)). This locality provides the ability to trace melt migration through the lithosphere and to investigate processes involved in creating oceanic crust ([Dick et al. 2008](#)). The core complex consists of numerous long-lived detachment faults forming uplifted, striated domes sub-parallel to the MAR and perpendicular to the Kane Fracture Zone ([Lissenberg and Dick 2008, Dick et al. 2008](#)). The associated first order segment of the MAR is a slow spreading center producing dominantly N-MORBs which show evidence for decreasing mantle potential-temperature towards the Kane transform wall ([Bryan et al. 1981](#)). The Kane OCC was sampled in 2004 on the KNR cruise 180-2 ([Tivey et al., 2004](#)). Samples were collected via dredging and remote controlled submersible Jason II. A very large and

detailed petrologic data set has been assembled (e.g. [Dick et al. 2006, 2008, 2010](#), [Lissenberg and Dick 2008](#)). Twenty-one samples for this study were selected based on detailed petrographic analysis, degree of alteration, spatial association, and relevance to the crustal creation process.

The distribution of rocks at the Kane OCC is not uniform, with gabbro found intruding into peridotite primarily in the southwest (Adam Dome) and northeast (Babel Dome) of the complex ([Dick et al. 2008](#)). The majority of gabbro samples for this study come from the Adam Dome and Cain Dome area (**Figure 1**). Seismic and petrologic evidence shows that multiple magmatic centers formed in the area ([Canales et al. 2008](#)) which is further evident in the temporal variation in degrees and rates of volcanic activity on the conjugate spreading plate ([Dick et al. 2008](#)). Adam Dome yielded the highest amount of primitive gabbro, and appears to have been fed through a conduit represented by a large, ~10 km wide zone of dunite ([Dick et al. 2008](#)). Primitive troctolite and gabbro at Adam Dome show evidence of significant melt-rock interaction, with oikocrysts of high Mg# (86-91) clinopyroxene forming in areas of melt impregnation and flow ([Lissenberg and Dick 2008](#)). The north and northeastern part of the OCC contain peridotite with large amounts of intruded melt, thereby forming massive outcrops of gabbroic rock ([Dick et al. 2008](#)). Rocks near Babel Dome are generally more evolved, typically occurring as oxide and olivine gabbro ([Dick et al. 2010](#)). The central region of the OCC contains a zone of very little intrusion, and largely yielded peridotite during sampling ([Dick et al. 2008](#)). Seismic evidence shows the presence of a large gabbroic body under the eastern side of Cain Dome, possibly related to either the expansion of the Babel Dome melt lens southward, or the location of a new magmatic center ([Canales et al. 2008](#), [Dick et al. 2010](#)).

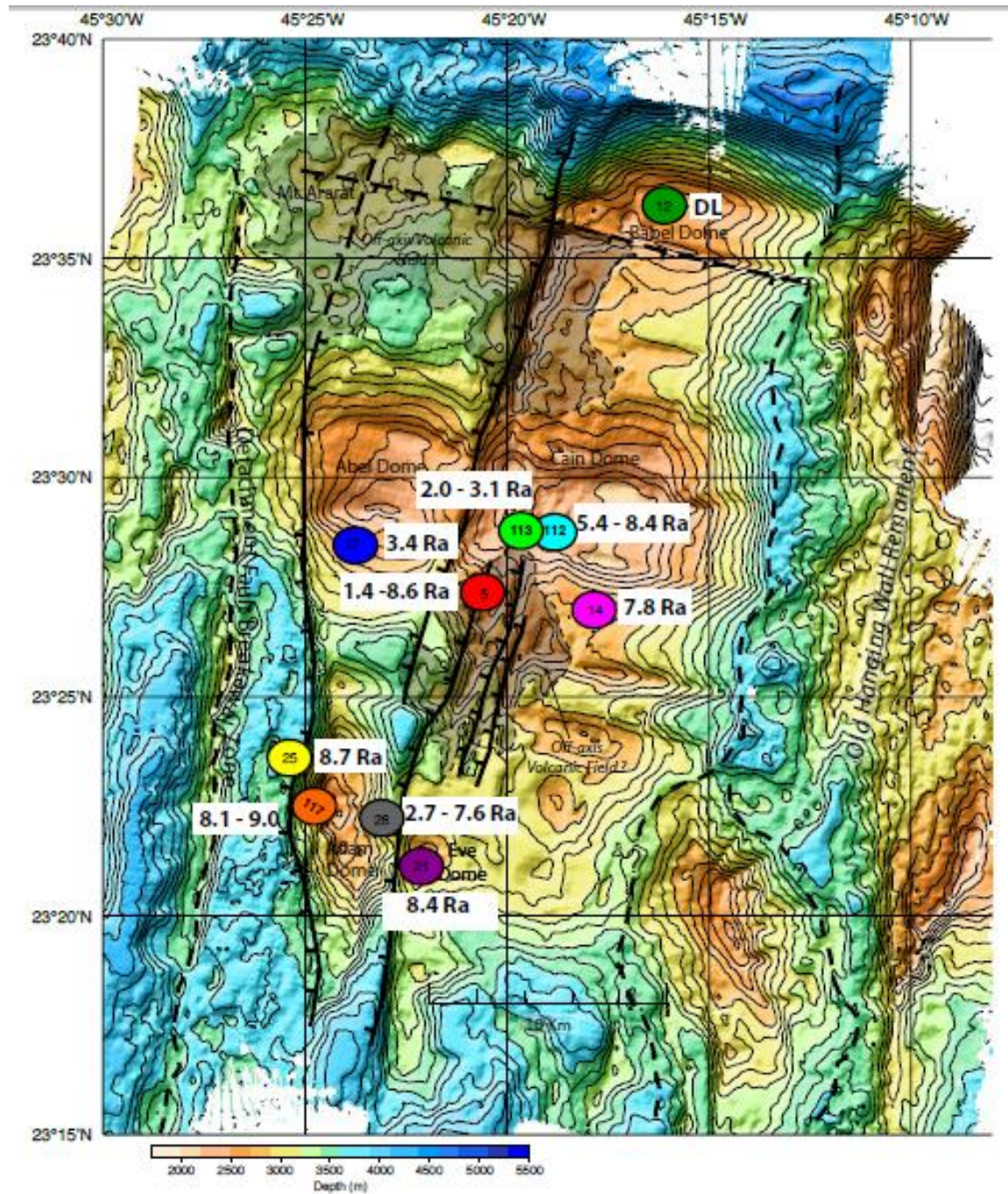


Figure 1: Map of the Kane OCC area modified from [Dick et al. \(2008\)](#). Locations of the sample dredge (two numbers) and dive (three numbers) sites are labeled and colored. Helium isotope ratios are shown in white boxes and represent the range of total melted $^3\text{He}/^4\text{He}$ sampled from each site (see discussion in text). DL stands for detection limited measurement. Contour intervals are 100 m.

A suite of troctolites collected along Adam Dome show considerable late-stage melt-rock interaction (*Lissenberg and Dick 2008*). There are two distinct types of clinopyroxene in these rocks. Type I clinopyroxene occurs as an oikocryst with a range of interstitial chadacrysts (olivine, plagioclase, spinel). These clinopyroxenes are generally finer grained than type II, averaging 2-8 mm in diameter. Type II clinopyroxenes are larger in diameter (up to 5 cm) and contain only plagioclase as chadacrysts. Both types of clinopyroxene are found within troctolite hosts, with type I occurring as interstitial grains mixed into the host rock while type II is primarily found as veins of gabbro through the troctolite hosts. Both types of clinopyroxene show anomalously high Mg#, ranging from 86-91 (with type I being slightly more Mg-rich). The high Mg#, combined with Cr₂O₃ contents (close to that of a primitive mantle melt) and oikocrystic structure (showing a separate stage of crystallization after the host rock crystallized) provide evidence for low-pressure recrystallization of both types of clinopyroxene. These samples therefore carry fundamental information on the relationship between melt and the country rock. Nevertheless, to explain their high clinopyroxene Mg# (a) MgO and Al₂O₃ were stripped from the country rock, resulting in a basaltic melt having lower CaO and SiO₂ and elevated MgO and Al₂O₃, or (b) melt was trapped in the upper crust, and clinopyroxene crystallized at the expense of the surrounding plagioclase, spinel, and olivine (*Lissenberg and Dick 2008*). Similar chemical co-variations are observed during high-pressure crystal fractionation of MORBs (e.g. *Constantin et al. 1996*); therefore additional work still is needed in order to distinguish between these two processes.

2. QUESTIONS ADDRESSED BY THIS STUDY

1. Are MORBs representative of isotopic variability in the upper mantle?
2. Is the entire spectrum of upper mantle heterogeneity represented by MORBs?

3. What can helium isotopes tell us about the magmatic history of the Kane area of the Mid-Atlantic Ridge?

3. SAMPLING and METHODS

3.1 Rock sampling:

Twenty-two crustal rock samples from the Kane OCC and eight basalt glasses from the nearby MAR were selected for this study (**Table 1**). Fresh rocks were chosen as much as possible based on petrographic observations, and an attempt was made to obtain a relatively large spatial distribution across the OCC of different rock types relevant to the crustal accretion process. The Kane OCC samples in this study were collected both by dredging and by submersible (JASON dives 112, 113, and 117) during the KNR 180-2 expedition. The eight MORB glasses are from the nearby MAR at 23°-24°N and were previously analyzed by [Bryan *et al.* \(1981\)](#) for major and trace elements, and by [Machado *et al.* \(1982\)](#) for Sr and Nd isotopes.

Rock samples were cored using a diamond drill bit. Typical whole rock sample sizes used for analysis were ~200-600 mg. Mineralogically heterogeneous samples were cored multiple times in an attempt to help characterize the distribution of helium throughout the rock. When possible, specific mineral phases in a sample were also hand-picked using a binocular microscope, to further constrain the location of He in the rocks. Samples were cleaned by physical scraping under a binocular microscope, followed by ultra-sonic cleaning in ethanol for 10 minutes, then two separate acetone baths for 15 minutes separated by acetone rinsing. Samples were then air-dried prior to gas extraction and helium isotope analysis.

Basalt glass was prepared in a manner similar to whole rock experiments with an increased amount of physical scraping in order to clean samples. The glass quality for the samples G104 17-13 and G104 2-1 was generally poor, with only low volume platey shards

available from the archive. The lower helium concentration of these two samples may be a factor of glass quality and not eruption history. Other samples provided good quality glass. More information on glass quality and phenocrystic abundances are provided in the appendix.

Table 1:
Sample lithology and location

Sample	Lithology/Rock Type	Latitude (°N)	Longitude (°W)	Depth(m)	Location
AII96 8-2	MORB Glass	24.001	46.184	2860-2212	N. Wall Kane Fracture Zone: Near Rift Intersection
AII96 18-1, 2	MORB Glass	23.517	44.817	3686-3573	S. Rift Valley: Kane Fracture Zone Intersections
G104 2-1	MORB Glass	24.151	46.267	3970-3800	N. Rift Valley: Kane Fracture Zone Intersection
G104 17-13	MORB Glass	23.617	42.034	4820-4410	S. Wall Kane Fracture Zone: Near Rift Intersection
G104 20-21	MORB Glass	23.619	45.034	4380-3820	S. Wall Kane Fracture Zone: Near Rift Intersection
G104 25-2, 3	MORB Glass	23.533	44.95	4560-4300	S. Rift Valley: Kane Fracture Zone Intersections
KNR 180-2 14-18 (1)	Olivine Gabbro	23.461	45.306	2453	Cain Dome
KNR 180-2 14-18 (2)	Plagioclase Vein	23.461	45.306	2453	Cain Dome
KNR 180-2 5-30	Oxide Gabbro Mylonite	23.471	45.358	2506	Cain Dome
KNR 180-2, 28-9	Olivine Gabbro Vein	23.383	45.382	2727	Adam Dome
Jas 113-20	Oxide Olivine Gabbro	23.471	45.359	Submersible	Cain Dome

Sample	Lithology/Rock Type	Latitude (°N)	Longitude (°W)	Depth(m)	Location
Jas 113-59b (3)	Gabbro-Nortite Vein	23.471	45.359	Submersible	Cain Dome
KNR 180-2 21-12	Troctolite	23.364	45.377	2880	Eve Dome
Jas 117-61	Troctolite	22.367	45.415	2400-3400	Adam Dome
Jas 117-62 (1)	Troctolite Host	22.367	45.415	2400-3400	Adam Dome
Jas 117-62 (2)	Gabbro Vein	22.367	45.415	2400-3400	Adam Dome
Jas 117-63 (1)	Troctolite Host	22.367	45.415	2400-3400	Adam Dome
Jas 117-63 (2)	Gabbro Vein	22.367	45.415	2400-3400	Adam Dome
KNR 180-2 25-1	Troctolite	23.395	45.415	2706	Adam Dome
KNR 180-2 5-31	Olivine Websterite	23.471	45.358	2506	Cain Dome
Jas 112-64	Orthopyroxenite	23.477	45.350	Submersible	Cain Dome
KNR 180-2 28-34	Harzburgite	23.383	45.382	2727	Adam Dome
Jas 112-84	Porphyroclastic Harzburgite	23.477	45.350	Submersible	Cain Dome
Jas 113-35	Harzburgite	23.471	45.359	Submersible	Cain Dome
JAS 112-49	Harzburgite	23.477	45.350	Submersible	Cain Dome
Jas 113-59a	Mylonitized Harzburgite	23.471	45.359	Submersible	Cain Dome
Jas 113-59b (1)	Mylonitized Harzburgite	23.471	45.359	Submersible	Cain Dome

Sample	Lithology/Rock Type	Latitude (°N)	Longitude (°W)	Depth(m)	Location
Jas 113-59b (2)	Serpentinized Dunite Vein	23.471	45.359	Submersible	Cain Dome
Jas 113-59b (4)	Talco-gouge	23.471	45.359	Submersible	Cain Dome
Jas 113-59b (5)	Mylonitized Harzburgite	23.471	45.359	Submersible	Cain Dome
KNR 180-2 12-5	Harzburgite	23.607	45.286	2282	Babel Dome
KNR 180-2 17-18	Mylonitized Spinel Harzburgite	23.480	45.384	2128	Abel Dome

Detailed information, including Jason II submersible dive cross-sections, is given in [Dick et al. \(2008\)](#) for Kane OCC rocks. Information for the basalt glasses is given in [Bryan et al. \(1981\)](#) and [Machado et al \(1981\)](#).

3.2 Helium isotope analyses

Whole rock samples, mineral separates and glasses were analyzed by a combination of methods, including crushing in vacuum, incremental heating, and total fusion using a high vacuum rock furnace. Samples designated in **table 2** with a † or * symbol indicate that the sample was heated at 50°C or 100°C overnight while pumping, prior to crushing analysis. This procedure was used in the case of several samples, in an attempt to drive off excess water prior to gas extraction, as the high degree of serpentinization in particular samples degraded our ability to achieve good vacuum in the extraction line even when pumping times were extended to several days.

Samples were loaded into a stainless steel tube, beneath a stainless magnetic piston, wherein they were crushed *in vacuo* at pressures of 10^{-7} to 10^{-6} torr. As mentioned above, in some cases the tubes were wrapped with a heating sleeve to bake the samples overnight under vacuum. Samples were repeatedly crushed by raising and dropping the magnetic piston on the

sample 75 times using a computer-controlled series of solenoids. This procedure liberates trapped gas including He and CO₂ in inclusions (melt and/or fluid), defects and along grain boundaries. The liberated CO₂ was trapped at liquid N₂ (77 K) temperature in a ‘U-trap’ during the crushing, and after processing of noble gases its partial pressure was measured using a high precision capacitance manometer (MKS, baratron, 1 torr) in a section of the line having a known calibrated volume. Other active gases not condensed at 77 K were removed using a sequence of SAES (Zr-Al alloy) “getters” (the first initially at 400°C and then allowed to cool during the sample processing and the second held at room temperature). Helium, neon and argon were ‘cryo-sorbed’ onto activated charcoal at 10 K in a Janis cryostat. After noble gas drawdown was complete (~25 minutes total processing time), the cryostat was warmed to 45 K to release the helium but retain the Ne and Ar. The helium was then admitted directly into a Nu instruments Noblesse model mass spectrometer.

Samples were also analyzed using an on-line furnace extraction system. Samples were step heated at 600°C, 1100°C, and 1600°C for 20 minutes per step after dropping them into a tantalum crucible. Selected mineral separates were also analyzed by total fusion at 1600°C for 20 minutes. Samples were cooled to 200°C before exposure to the hot getter, thereafter samples were processed in the same manner as the crushing extractions (CO₂ was not measured during furnace runs because it reacts with the hot metal surfaces). Hot blanks were run at 1650°C between samples to assure complete extraction of He from the previous sample. No significant difference between hot and cold blanks was detected during this study. An initial batch of samples was processed as total fusion steps at 1400°C due to temperature instability in the furnace at higher temperatures. Although hot blanks at 1450°C proved low, later analysis at 1600°C showed that some of these samples suffered incomplete extraction of He. While this

initial batch of data contains useful information, our discussion of the overall results from this study is focused on the second batch of data.

$^3\text{He}/^4\text{He}$ was measured using a Nu Instruments Noblesse model mass spectrometer operated in static mode, using magnetic field peak switching. Line blanks were run before each sample analysis, and the measured ^3He and ^4He in all samples were blank corrected. Typically blanks were $< 1 \times 10^{-10}$ ccSTP for ^4He . Numerous aliquots of HESJ (Helium Standard of Japan; [Matsuda et al. 2002](#)) were analyzed throughout this study, mostly overnight under computer automation. Our HESJ standard is a split of the same gas used in the helium isotope lab at NOAA/PMEL in Newport, OR. It has a $^3\text{He}/^4\text{He}$ of 20.4 R_A , determined in the OSU lab compared to marine air collected in 2007, which is in complete agreement with the value reported by [Lupton and Evans \(2004\)](#). For gabbro and peridotite sample sizes typically analyzed in this study, the reproducibility of the HESJ $^3\text{He}/^4\text{He}$ was $\pm 1\%$ (1σ). For basalt glasses the standard reproducibility was typically $\pm 0.25\%$ (1σ). Although some samples contained large concentrations of $\text{H}[^2\text{H}]$ (HD) upon inlet into the mass spectrometer, there was no observable effects on the centered peak locations where ^3He was measured. Furthermore, during analysis the HD concentration exponentially decreased due to exposure to a high temperature ‘getter’ in the mass spectrometer while the ^3He concentrations showed no correlated effects.

Table 2.
Helium Isotope and He and CO₂ Concentrations for Rocks from the Kane OCC and Adjacent Ridge Axis

Sample	Type	Weight mg	Extraction	⁴ He 10 ⁻⁹ ccSTP/g	³ He 10 ⁻¹⁵ ccSTP/g	³ He/ ⁴ He R/R _A	2σ	[CO ₂] 10 ⁻³ ccSTP/g	³ He/ ⁴ He [³ He] _c / [³ He] _t
Basalt Glass									
AII96 8-2	glass chips	158.6	cr	16988	197873	8.38	0.05	243	
AII96 18-1	glass chips	273.2	cr	20866	252571.0	8.71	0.05	137	
	glass chips	166.3	1400	13083	156886.6	8.63	0.07		
AII96 18-2	glass chips	266.2	cr	17656	212477.3	8.66	0.06	100	
G104 2-1	glass chips	124.6	cr	1811	21404	8.50	0.07	7.68	
G104 17-13	glass chips	118.6	cr	1386	16344	8.49	0.10	29.8	
G104 20-21	glass chips	183.0	cr	1654	19045	8.28	0.10	87.6	
G104 25-2	glass chips	230.5	cr	1148	13837.1	8.67	0.07	183	
G104 25-3	glass chips	280.9	cr	9600	116243.7	8.71	0.06	198	
	glass chips	218.0	1400	7130	86154.8	8.69	0.08		
Gabbro									
KNR180-2 14-18(1) a*	wr	537.7	cr	1.54	9.4	4.39	0.37	DL	0.06
KNR180-2 14-18(1) b	wr	608.0	cr	1.10	8.1	5.31	0.47	21.4	0.05
KNR180-2 14-18(1)	wr	324.2	600	DL	DL	DL	-		
			1100	0.96	7.2	5.45	0.84		
			1600	12.94	142.5	7.92	0.41		
			calc total	13.90	149.8	7.75	0.40		
KNR180-2 14-18(2)*	wr	529.6	cr	0.57	DL	DL	-	DL	
KNR180-2 5-30	wr	633.6	cr	2.65	22.1	5.99	0.34	DL	0.46

Sample	Type	Weight mg	Extraction	^4He 10^{-9} ccSTP/g	^3He 10^{-15} ccSTP/g	$^3\text{He}/^4\text{He}$ R/R _A	2σ	$[\text{CO}_2]$ 10^{-3} ccSTP/g	$\frac{^3\text{He}_c}{^3\text{He}_t}$
KNR180-2 5-30	wr	177.8	600	1.33	DL	DL	-		
			1100	17.97	23.0	0.92	0.11		
			1600	4.34	24.1	3.99	0.48		
			calc total	23.64	47.6	1.45	0.17		
KNR180-2 5-30	amph	103.8	cr	27.85	305.6	7.90	0.33	1.52	0.43
KNR180-2 5-30	amph	32.5	1600	114.73	715.0	4.48	0.27	12.1	0.14
KNR180-2 5-30	cpx	611.1	cr	2.42	23.1	6.89	0.39		
KNR180-2 5-30	cpx	387.6	600	2.41	14.9	4.43	0.49		
			1100	15.98	138.6	6.24	0.31		
			1600	DL	7.0	DL	-		
			calc total	18.88	160.5	6.11	0.30		
KNR180-2 28-9	wr	542.5	cr	1.63	5.2	2.31	0.30	0.626	0.01
KNR180-2 28-9	wr	216.6	600	DL	DL	DL	-		
			1100	7.07	44.1	4.49	0.41		
			1600	56.95	602.2	7.61	0.21		
			calc total	64.10	646.4	7.26	0.29		
JAS113-20*	wr	501.5	cr	0.95	5.0	3.80	0.40	0.590	
JAS113-20	wr	707	1400	DL	DL	DL	-	DL	
JAS113-20*	cpx	667.6	cr	DL	DL	DL	-		
JAS113-59b(3)a*	wr	555.2	cr	2.11	8.0	2.72	0.24	0.666	0.08
JAS113-59b(3)b	wr	343.1	cr	1.60	15.9	7.15	0.59	5.79	0.17
JAS113-59b(3)	wr	494.5	600	13.62	39.8	2.10	0.13		
			1100	7.83	46.9	4.31	0.28		
			1600	0.65	8.7	9.61	1.09		
			calc total	22.10	95.4	3.11	0.34		

Sample	Type	Weight mg	Extraction	^4He 10^{-9} ccSTP/g	^3He 10^{-15} ccSTP/g	$^3\text{He}/^4\text{He}$ R/R _A	2 σ	$[\text{CO}_2]$ 10^{-3} ccSTP/g	$\frac{^3\text{He}_c}{^3\text{He}_t}$
Troctolite									
KNR180-2 21-12	wr	555.2	cr	3.15	16.6	3.78	0.26	0.581	0.09
KNR180-2 21-12	wr	303.5	600	0.41	6.3	11.18	1.63		
			1100	3.13	29.1	6.68	0.56		
			1600	11.52	140.2	8.75	0.44		
			calc total	15.06	175.6	8.39	0.42		
JAS117-61a	wr	529.7	cr	44.99	560.1	8.96	0.22	0.138	0.21
JAS117-61b†	wr	474.8	cr	17.69	208.8	8.49	0.19	DL	0.08
JAS117-61	wr	256.1	600	3.63	37.3	7.40	0.68		
			1100	49.25	613.7	8.96	0.23		
			1600	164.66	2059.7	9.00	0.14		
			calc total	214.14	2676.8	8.99	0.17		
JAS117-62(1)	wr	564.5	cr	0.62	DL	DL	-	1.42	0.10
JAS117-62(1)	wr	525.8	600	1.07	8.9	5.94	0.76		
			1100	0.92	10.1	7.83	0.89		
			1600	4.35	53.2	8.79	0.49		
			calc total	6.35	72.1	8.17	0.46		
JAS117-62(2)	wr	366.1	cr	0.38	DL	DL	-	0.150	0.05
JAS117-62(2)	cpx	207.7	cr	2.80	19.4	5.00	0.44	DL	
JAS117-62(2)	wr	348.5	600	0.86	DL	DL	-		
			1100	DL	DL	DL	-		
			1600	DL	DL	DL	-		
			calc total	0.86	DL	DL	-		
JAS117-63	wr	523.3	cr	0.69	3.5	3.65	0.44	DL	
JAS117-63(1)	wr	750.0	cr	0.98	10.2	7.51	0.64	0.529	
JAS117-63(2)	wr	567.6	cr	0.62	3.4	3.93	0.69	0.373	

Sample	Type	Weight mg	Extraction	^4He 10^{-9} ccSTP/g	^3He 10^{-15} ccSTP/g	$^3\text{He}/^4\text{He}$ R/R _A	2σ	[CO ₂] 10^{-3} ccSTP/g	$\frac{^3\text{He}_c}{^3\text{He}_t}$
KNR180-2 25-1	wr	535.2	cr	54.81	657.2	8.63	0.20	DL	0.46
KNR180-2 25-1	wr	273.2	600	2.57	13.0	3.64	0.47		
			1100	20.10	247.0	8.84	0.40		
			1600	96.32	1179.5	8.81	0.19		
			calc total	118.99	1439.5	8.70	0.19		
Ultramafic Veins									
KNR180-2 5-31	wr	500.4	cr	3.25	30.3	6.70	0.35	0.314	
KNR180-2 5-31	wr	440.7	1400	14.12	168.2	8.57	0.34		
KNR180-2 5-31	cpx	377.4	cr	1.38	11.8	6.11	0.56	4.42	
KNR180-2 5-31	opx	225.3	1600	18.90	202.4	7.70	0.38		
JAS112-64*	wr	575.6	cr	0.39	DL	DL	-	DL	
JAS112-64	wr	670.4	1400	1.75	DL	DL	-		
Peridotites									
KNR180-2 28-34	cpx	207.6	cr	4.15	36.2	6.28	0.47	1.69	0.22
KNR180-2 28-34	cpx	61.7	1600	43.98	162.7	2.66	0.22		
KNR180-2 28-34	opx	309.5	cr	3.04	24.6	5.82	0.40	1.48	0.15
KNR180-2 28-34	opx	185.1	1600	24.64	162.3	4.74	0.26		
JAS112-84a†	wr	455.0	cr	14.98	169.8	8.16	0.19	0.204	0.09
JAS112-84b	wr	704.3	cr	53.10	639.7	8.67	0.14	0.170	0.32
JAS112-84	wr	181.1	1100	50.32	591.3	8.45	0.25		
			1600	119.79	1391.1	8.36	0.19		
			calc total	170.37	1987.9	8.39	0.19		
JAS113-35	wr	441.1	cr	1.09	DL	DL	-	DL	
JAS113-35	opx	390.7	cr	0.33	DL	DL	-	DL	
JAS112-49	Wr	481.2	cr	0.92	DL	DL	-	DL	0.01

Sample	Type	Weight mg	Extraction	^4He 10^{-9} ccSTP/g	^3He 10^{-15} ccSTP/g	$^3\text{He}/^4\text{He}$ R/R_A	2σ	$[\text{CO}_2]$ 10^{-3} ccSTP/g	$\frac{^3\text{He}c}{^3\text{He}t}$
JAS112-49	Wr	256.6	600	4.70	57.1	8.74	0.75		
			1100	3.96	7.6	1.39	0.18		
			1600	0.24	DL	DL	-		
			calc total	8.89	66.7	5.40	0.46		
JAS113-59a†	Wr	532.1	cr	DL	DL	DL	-	0.156	0.00
JAS113-59a	Wr	405.2	600	4.37	31.3	5.15	0.48		
			1100	8.10	DL	DL	-		
			1600	DL	DL	DL	-		
			calc total	12.60	31.3	2.09	0.19		
JAS113-59b(1)†	wr	582.2	cr	DL	DL	DL	-	DL	
JAS113-59b(2)†	wr	682.4	cr	DL	DL	DL	-	0.108	
JAS113-59b(4)†	wr	543.6	cr	DL	DL	DL	-	5.32	
JAS113-59b(5)†	wr	633.9	cr	DL	DL	DL	-	2.36	
KNR180-2 12-5†	wr	407.9	cr	0.25	DL	DL	-	2.21	
KNR180-2 12-5	opx	228.3	cr	DL	DL	DL	-	0.442	
KNR180-2 17-18†	wr	539.3	cr	1.05	7.6	5.22	0.50	5.17	0.08
KNR180-2 17-18	wr	447.8	600	7.05	44.5	4.54	0.31		
			1100	12.52	48.4	2.78	0.18		
			1600	1.01	DL	DL	-		
			calc total	20.58	96.2	3.36	0.22		

$^3\text{He}/^4\text{He}$ is reported as R/R_A , where R_A is the atmospheric ratio (1.39×10^{-6}).

$[^3\text{He}]c / [^3\text{He}]t$ denotes the ratio of ^3He calculated in the crushed extraction versus the total melt extraction.

† indicates the sample was baked at 50°C overnight

* indicates the sample was baked at 100°C overnight.

wr = whole rock; cpx = clinopyroxene; opx = orthopyroxene; amph = amphibole.

cr = extraction by crushing ; 600, 1100 and 1600 denote incremental heating extractions (°C). Other reported temperatures are single total fusion analyses.

DL= below detection limited; defined here as three times the uncertainty in the blank for ^4He and ^3He . For CO_2 DL was taken as less than 1.0×10^{-4} cc/g.

Letters a, b following samples denotes different whole rock cores from the same sample.

3.3 Microprobe and laser ablation analyses

Electron microprobe analyses were performed on clinopyroxene, orthopyroxene, and amphibole separates from samples JAS 113-20, KNR-180-2 5-30 and KNR 180-2 14-18. These data allow us to fill in some gaps from the original work done in [Dick et al. \(2010\)](#). Mineral separates retrieved from the crushed rocks following the He analysis were also analyzed in an attempt to fully characterize the composition/classification of the minerals. These remaining partially crushed minerals in the powders were polished to 1 μm roughness in a grain mount and analyzed using the Cameca SX-100 electron microprobe at OSU.

Subsets of mineral separates were also analyzed for the trace elements; Li, Rb, Sr, Y, Zr, Nb, Ba, the REEs, Pb, U, and Th (**Table 3**). Samples were ablated using a Photon Machines Analyte G2 nm ArF “fast” Excimer Laser and elemental concentrations were determined using a thermal x-series 2 ICP-MS. Samples were run using an 85 μm spot size with a laser output of 70% and a fluence of 4.84 J/cm². Ten analysis were taken for each mineral type on three to four separate grains. Background concentrations were collected for 30 seconds prior to each analysis. Standards were run before, after, and during the batch runs and included the USGS basaltic glass standards GSE-1G, GSD-1G, BHVO-2G, and BCR-2G. Typical uncertainty for each standard ranged from 0.5 to 1.7% (1 SE). Concentrations were internally normalized to Ca, measured independently using the electron microprobe, to account for matrix effects or ablation rate.

Table 3:
Select major and trace element data:

	KNR180 -2 14-18 CPX	KNR180 -2 14-18 AMP	KNR180 -2 5-30 CPX	KNR180 -2 5-30 AMP	JAS113 -20 CPX	JAS113 -59b(3) CPX†	KNR180 -2 5-31 CPX	KNR180 -2 5-31 OPX	JAS112 -84 OPX†	KNR180 -2 28-34 CPX	KNR180 -2 28-34 OPX
Major element data (weight %)											
SiO₂	54.78	51.05	52.91	46.59	52.46	51.22	52.93	55.95	54.95	52.03	54.56
Al₂O₃	0.66	5.91	2.05	8.25	3.06	2.78	4.30	3.94	3.89	5.50	4.12
K₂O	0.003	0.14	0.005	0.15	0.01		0.03	0.004		0.004	0.004
FeO	5.92	7.78	10.33	14.26	8.15	10.56	3.33	7.08	6.08	3.45	5.74
Na₂O	0.32	1.75	0.48	2.38	0.41	0.45	0.37	0.01	0.02	0.04	0.00
MgO	16.95	19.10	15.81	14.44	15.92	15.39	18.53	32.74	32.80	18.00	31.95
Cr₂O₃	0.03	0.03	0.01	0.01	0.18	0.03	1.37	0.99	0.79	1.38	0.98
TiO₂	0.06	1.45	0.46	2.50	0.65	0.82	0.09	0.04	0.05	0.09	0.04
CaO	20.53	11.09	17.72	10.28	18.83	17.64	17.79	1.51	1.95	19.28	2.09
NiO	0.02		0.03		0.04		0.09	0.11		0.07	0.11
Total	99.3	98.3	99.8	99.0	99.7	99.2	98.8	102.3	100.6	99.7	99.9
Trace element data (ppm)											
La	46.6	4.30	0.59	23.9	0.20	-	-	-	-	-	-
Ce	316	17.2	3.26	157	1.52	1.37	-	-	-	-	-
Pr	63.1	2.30	0.66	37.1	0.38	0.33	-	-	-	-	-
Nd	379	10.5	4.23	270	3.10	1.87	-	0.032	-	-	-
Sm	137	2.70	1.87	123	1.72	1.21	-	-	0.006	-	-
Eu	13.8	1.26	0.81	20.9	0.65	0.53	-	-	-	0.032	-
Gd	184	3.08	3.18	179	3.23	2.38	0.50	-	-	0.248	-
Tb	31.9	0.51	0.58	30.5	0.60	0.50	0.12	-	0.006	0.065	-
Dy	230	3.51	4.50	218	4.42	4.42	1.05	-	0.072	0.620	0.059
Ho	47.5	0.70	0.96	43.0	0.94	1.06	0.23	-	0.024	0.144	0.023
Er	153	2.32	2.89	128	2.90	4.25	0.81	-	0.118	0.553	0.106
Tm	19.2	0.30	0.38	15.1	0.37	0.65	0.11	-	0.017	0.073	0.020
Yb	127	2.20	2.70	96.3	2.45	5.58	0.72	0.291	0.176	0.548	0.186
Lu	17.6	0.32	0.38	12.6	0.37	0.85	0.11	0.052	0.032	0.082	0.034
Th	0.037	0.128	0.014	0.013	-	0.010	-	-	-	-	-
U	0.007	0.069	0.015	0.008	-	0.140	-	-	-	-	-

† indicates major element data is from Dick et. al. (2010). All other data is new to this study.

- Indicates either the measurement was below detection limit or uncertainty in the measurement is greater than 40%

Uncertainty in major element measurements is generally 1 - 5%.

For REEs, gabbroic clinopyroxene and amphibole vary from 3-15% uncertainty while peridotite clinopyroxene and orthopyroxene varies from 10-39%.

U & Th measurements contain an uncertainty between 10 – 20% where listed.

4 RESULTS

Helium and CO₂ data are reported in **Table 2**. Major element data for selected samples are reported in **Table 3** while the remaining major element data for our sample set are available in [Dick et al. \(2010\)](#) and [Lissenberg and Dick \(2008\)](#). Major and trace element data for the basalts are reported in [Bryan et al. \(1981\)](#), and Sr and Nd isotopic data are reported in [Machado et al. \(1981\)](#).

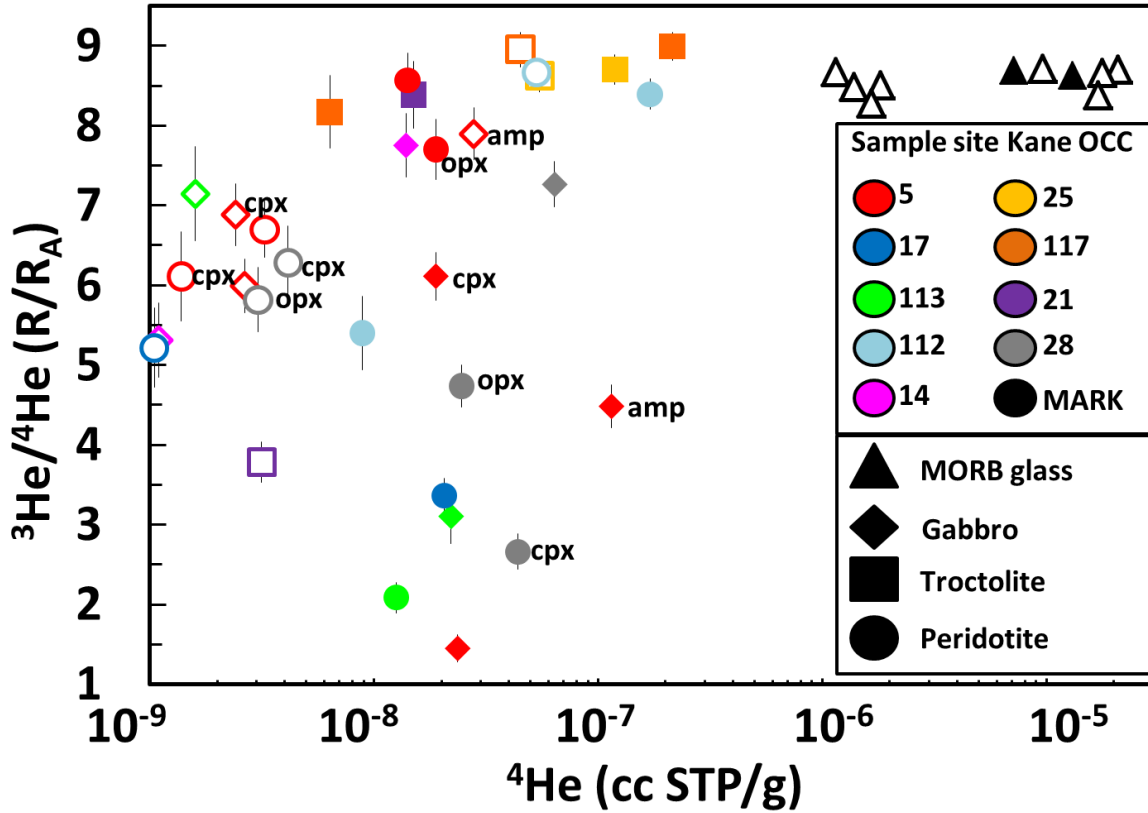


Figure 2: $^3\text{He}/^4\text{He}$ is plotted as R/R_A , where R_A is the atmospheric ratio (1.39×10^{-6}). ^4He concentration is plotted as ccSTP/g. Calculated total fusion values are plotted using filled symbols. *Note: the total melt value may not be representative of the primary magmatic value, many fresh samples contain higher $^3\text{He}/^4\text{He}$ values at the 1600°C step than the total melted value, see **Table 1**. Hollow symbols represent crushed extractions. Only non-baked results are plotted for repeated crushing experiments. Mineral separates are labeled to the left of the symbol. Cpx= clinopyroxene; Opx= orthopyroxene; Amp=Amphibole. Error bars are displayed as $\pm 2\sigma$

Figure 2 shows $^3\text{He}/^4\text{He}$ versus $[\text{He}]$ (ccSTP/g) of the full data set. Several important observations can be made:

1. The highest He contents occur in the basalt glasses. The range of observed values is a factor of 10-1000 times higher than in gabbroic and ultramafic rocks from the Kane OCC.
2. A narrow range of $^3\text{He}/^4\text{He}$ is observed in the basalts, between 8.4 and 8.7 R_A .
3. $^3\text{He}/^4\text{He}$ ratios between ~ 7 and 9 R_A , typical of the global range of MORBs away from high ^3He hotspots ([Graham 2002](#)), are observed in a number of peridotite, gabbro and troctolite samples, despite their low $[\text{He}]$ compared to the glasses.
4. A large range in $^3\text{He}/^4\text{He}$, trending to lower ratios, is observed in a number of samples, and this typically occurs at $[\text{He}]$ below 10^{-7} cc STP/g.

These observations are discussed in more detail below for the range of rock types analyzed in this work.

4.1 Basalts:

Due to their poor degree of preservation, no basalts collected from the Kane OCC itself were analyzed in this study. Eight basalt glasses collected near the northern and southern intersections of the Mid-Atlantic Ridge with the Kane Fracture Zone were selected for analysis, in order to provide a context for the mantle-derived $^3\text{He}/^4\text{He}$ signal in the Kane area. These basalt glasses show a relatively narrow range of $^3\text{He}/^4\text{He}$ ratio, between 8.4 and 8.7 R_A (**Table 2**), and relatively high He concentrations. Helium concentrations in the glasses range between 1 and 21 $\mu\text{cc STP/g}$, and there is no systematic variation of $^3\text{He}/^4\text{He}$ with $[\text{He}]$ (**Figure 1**). The basalts with the highest $^3\text{He}/^4\text{He}$ (AII96-18 and G104-25) were recovered from the southern intersection of the MAR and Kane FZ. These samples are also characterized by some of the most radiogenic $^{143}\text{Nd}/^{144}\text{Nd}$ and least radiogenic $^{87}\text{Sr}/^{86}\text{Sr}$ values for MORBs globally (ϵNd up to +14 and

$^{87}\text{Sr}/^{86}\text{Sr}$ down to 0.7022). The similarity of the two samples analyzed from each of these dredges may indicate that they sampled the same, or closely related, lava flow units.

The amount of helium released by crushing of the basalts varies with the amount of vesicle carbon dioxide (**Table 2**), as expected for the relatively small range of $\text{CO}_2/{}^3\text{He}$ in MORBs (e.g., *Marty and Jambon 1987; Marty and Zimmerman 1999*). The range of $\text{CO}_2/{}^3\text{He}$ measured in the Kane MORB glasses is $3.6 \times 10^8 - 1.3 \times 10^{10}$. The lower concentrations seen in samples G104 17-13 and G104 2-1 (1.4 and 1.6 $\mu\text{cc STP/g}$ respectively) may be a factor of the high surface area, platey glass used and not necessarily related to eruptive processes or source chemistry. See the appendix for more information on glass quality for each basalt.

4.2 Ultramafic rocks:

The porphyroclastic harzburgite JAS112-84 contains relatively high [He] when crushed (53 ncc STP/g) and during melting analysis (170 ncc STP/g). This rock is comprised of relatively fresh olivine, with parallel lines of fluid inclusions that appear to indicate high temperature annealing (*Natland 2003*) (**Appendix Figure A1(b)**). When step heated, 58% of the He in this sample was released during the 1600°C temperature (fusion) step, indicating that much of the He reside in either the crystal lattice or in small fluid inclusions in olivine. There was a moderate variability in the isotopic ratio as indicated by the three different ${}^3\text{He}/{}^4\text{He}$ values during two crushing analyses (8.1 ± 0.2 , $8.6 \pm 0.1 R_A$) and a single step heating analysis ($8.4 \pm 0.2 R_A$ total). Sample JAS 112-84a was crushed after the sample was baked overnight at 50°C, and this analysis had 72% less He and a lower ${}^3\text{He}/{}^4\text{He}$ ratio than the unbaked sample JAS 112-84b. It is unclear whether this difference is due to sample heterogeneity, the baking procedure or a combination of both. Only 31% of the He contained in this sample was released through crushing

indicating that the majority of its He is probably contained in the crystal lattice, or in very tiny inclusions that could not be ruptured by our crushing procedure.

The highly oxidized harzburgite sample KNR 180-2 28-34 contained surprisingly clean orthopyroxene and clinopyroxene crystals in a matrix of orange oxidized clay. When crushed these minerals had relatively low [He] at 4.2 ncc STP/g (clinopyroxene) and 3.0 ncc STP/g (orthopyroxene), and the trend shows lowered $^3\text{He}/^4\text{He}$ values relative to MORB glasses (**Figure 2**). The majority of He in these samples (~90%) is released during total fusion, wherein the effects of radiogenic He in pyroxene can be clearly seen. The clinopyroxene in this sample shows a significant decrease in $^3\text{He}/^4\text{He}$ value, from $6.3 \pm 0.5 R_A$ (during crushing) to $2.7 \pm 0.2 R_A$ (during melting) while the orthopyroxene showed a corresponding decrease from $5.8 \pm 0.4 R_A$ to $4.7 \pm 0.3 R_A$. This is consistent with typical differences in the U and Th content of clinopyroxene vs. orthopyroxene, and may indicate that orthopyroxene in the harzburgites more faithfully tracks the primary He isotopic signature in these types of rocks after they are a few million years old.

All the mylonitic peridotites had relatively low $^3\text{He}/^4\text{He}$ ratios, but some had [^4He] concentrations up to 20 ncc STP/g when melted. The only sample which contained measurable He when crushed was a spinel harzburgite (KNR180-2 17-18), although the level was low (1 ncc STP/g). The mylonites released the majority of helium at lower temperatures (600°C, 1100°C) and have associated higher amounts of H₂O (seen from the increased background pressure in the extraction line) and H (as seen from the higher amounts of HD in the mass spectrometer).

The olivine websterite vein (KNR180-2 5-31) appears to be in chemical equilibrium with its harzburgite host and most likely formed *in situ* during mantle upwelling ([Dick et al. 2010](#)). This sample had $^3\text{He}/^4\text{He} = 8.6 \pm 0.3 R_A$ during total fusion (at 1400°C). Although this lower temperature analysis during the first sample batch runs likely provides a low estimate for the

total [He], the sample appears to be in isotopic equilibrium with the nearby harzburgite sample JAS112-84 (which had $^3\text{He}/^4\text{He}$ value of 8.4-8.7 R_A). The lower $^3\text{He}/^4\text{He}$ obtained for mineral separate analyses of clinopyroxene ($6.1 \pm 0.6 R_A$ crushed) and orthopyroxene ($7.7 \pm 0.4 R_A$ melted) in the olivine websterite may contain a small additional radiogenic component, which increases the ^4He and thus lowers the ratio. This also suggests that the fresh fine grain olivine dominates the whole rock He isotope signature in this sample.

The other ultramafic vein analyzed in this study was an orthopyroxenite (JAS112-64). Both crushing and fusion analysis of this sample suggest it is completely degassed in terms of ^3He with some small amount of radiogenic ^4He possibly released. While this may be due to processes associated with orthopyroxenite formation, it is also notable that this sample is characterized by the presence of a cross-cutting oxide gabbro vein which intruded through the orthopyroxenite at high temperature (*Dick et al. 2010*).

No lherzolites were available for this study, and no dunites were found to be fresh enough for helium isotope analysis.

4.3 Primitive gabbro (troctolite and troctolitic gabbro):

The primitive gabbros in this study consist of troctolites and troctolitic gabbros. These are mafic intrusive rocks dominated by olivine and plagioclase with minor amounts of pyroxene. Because their bulk chemical compositions do not correspond to partial melts of peridotite they are generally considered to be cumulate in origin. The troctolites in this study all come from submersible dives and dredges around Adam and Eve Domes (**Table 1**). The freshest troctolites (JAS117-61 and KNR180-2 25-1) are far from any notable intruded gabbro veins, and they contain trapped melt represented by clinopyroxene with an elevated Mg# (*Lissenberg and Dick 2008*). These samples contain some of the highest He concentrations measured in the Kane OCC,

as extracted from both crushing and melting experiments (214 and 120 ncc STP/g total fusion results, respectively). Between ~80 and 60% of the He in these whole rock samples was released during melting. The He is likely to dominantly reside in both olivine and clinopyroxene, as indicated by the presence of small fluid inclusions in these phases (**Appendix Figure AI(d)**) and the observation that the highest amounts of helium were released at 1600°C (with lesser amounts released at 1100°C; **Table 2**). The similar $^3\text{He}/^4\text{He}$ for helium released during the 1100°C and 1600°C steps for each of these two whole rock samples possibly indicates that the trapped melt (clinopyroxene) and the olivine are in isotopic equilibrium. The trend of decreasing $^3\text{He}/^4\text{He}$ with [He] observed in **Figure 3a** suggests a possible role for contamination by loosely bound radiogenic helium in JAS117-61 at low temperature (7.40 R_A and [He] = 3.6 ncc STP/g, at 600°C). Collectively the troctolite results suggest that the primary, mantle derived signature in these rocks is $\sim 9.0 \pm 0.2 R_A$.

Two other troctolite samples (JAS117-62, 63) contained gabbroic veins, and are described as type-2 bearing clinopyroxene veins in [Lissenberg and Dick \(2008\)](#). These gabbroic veins contained [He] which was near or below the detection limit during both crushing and melting analyses. A clinopyroxene separate from the gabbroic vein in JAS117-62(2) contained measureable He when crushed with a $^3\text{He}/^4\text{He}$ value of $5.0 \pm 0.4 R_A$ and [He] = 2.8 ncc STP/g. Furthermore, the troctolite host JAS117-62(1) contained increasing concentrations of He during step heating when samples were drilled ~1 cm away from any gabbroic vein. The measured $^3\text{He}/^4\text{He}$ of the 1600°C step was $8.8 \pm 0.2 R_A$ ([He] = 4.4 ncc STP/g) while the lower temperature steps contained less helium ($^3\text{He}/^4\text{He}$ of $5.9 \pm 0.7 R_A$, 1.0 ncc STP/g at (600°C) and $7.8 \pm 0.9 R_A$, 0.9 ncc STP/g at 1100°C).

Sample KNR180-2 21-12 was a highly serpentinized gabbroic troctolite from Eve Dome, and contained low [He] when crushed, as well as when heated at both 600°C and 1100°C. Notably, however, at the highest temperature step of 1600°C it released 12 ncc STP/g of He with a $^3\text{He}/^4\text{He}$ ratio of $8.7 \pm 0.4 R_A$. The ratio is consistent with other troctolites from southern Kane domes. **Figure 3c** shows the role of alteration potentially from seawater during serpentinization, on lowering the $^3\text{He}/^4\text{He}$ value of this sample.

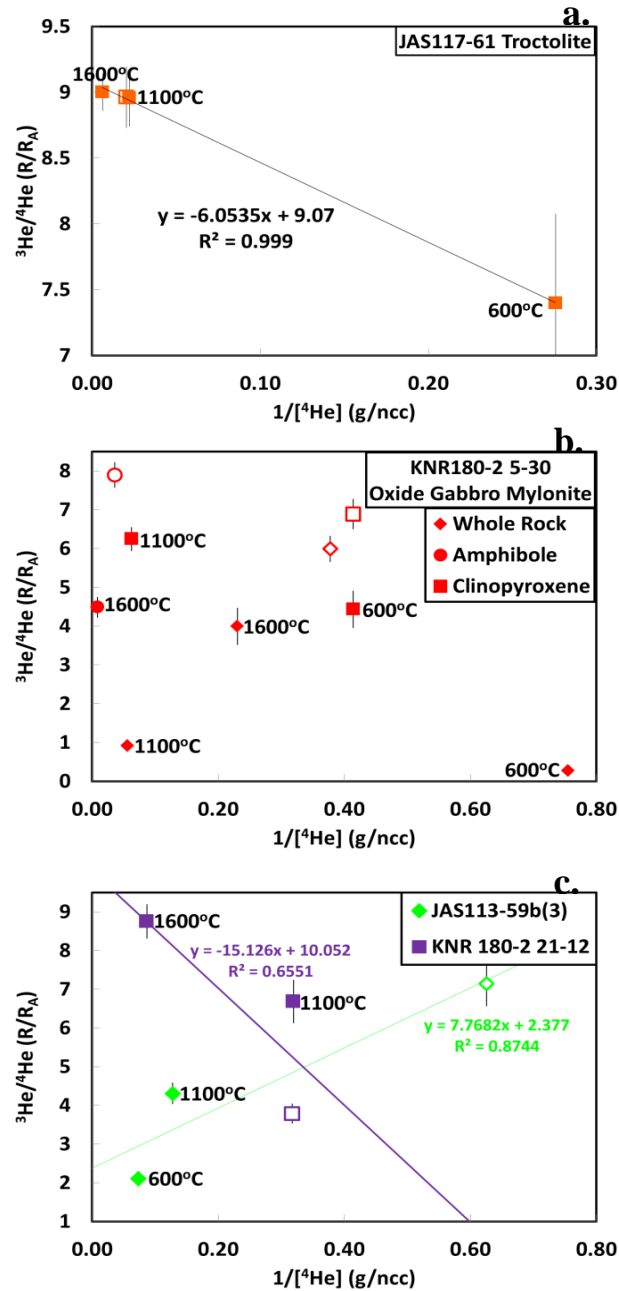


Figure 3: This chart shows $^3\text{He}/^4\text{He} (R/R_A)$ v. $1/[^4\text{He}] (\text{g/ncc})$ in order to show the source of potential contaminations on the helium signature. Colors represent location of the dredge/dive site (as shown in fig. 1). A.) JAS117-61 showing the potential role of atmospheric contamination reducing the primary $^3\text{He}/^4\text{He}$ value. B.) KNR180-2 5-30 shows the difficulty in some samples of separating the roles of radiogenic ingrowth, atmospheric contamination, and degassing. C.) Sample JAS113-59b(3) shows the effect of radiogenic ingrowth, most likely due to the relatively high U content of the clinopyroxene (0.14ppm). KNR180-2 21-12 shows the potential role of atmospheric(seawater) contamination in masking the primary signature in this heavily serpentinized troctolite.

4.4 Gabbro:

The less primitive gabbros in this study contain the largest degree of isotopic heterogeneity. In some cases the step heating plus fusion extractions, of whole rocks and separated minerals, appears to have resolved primary and secondary He isotope signatures in these rocks, but with varying degrees of success. For some samples the measured results undoubtedly reflect additions of radiogenic and/or seawater/hydrothermal components.

Two olivine gabbros (KNR180-2 14-18 and KNR180-2 28-9) were analyzed. Petrographic examination of sample 14-18 shows large concentrations of what appears to be metamorphic amphibole filling in shear zones. According to [Coogan et al. \(2001\)](#), a magmatic vs. hydrothermal genesis for amphibole can be discerned through the relative concentrations of Nb and differences in the Nb/La ratio. Fluids interacting with gabbroic suites are expected to be depleted in Nb while, due to the incompatible nature of Nb, highly evolved gabbroic melts are likely to be enriched. Thus, it is expected that hydrothermally formed amphibole will be depleted in Nb while magmatic amphibole will be enriched in Nb. The KNR 180-2 14-18 amphibole contains nearly undetectable Nb concentrations of 0.35 ± 0.15 ppm (**Table 3**) indicating a hydrothermal origin for the amphibole. Texturally the amphibole is found as clusters of grains within shear zones which further support a hydrothermal origin. The clinopyroxene in the same sample appears to have formed from igneous processes and contains a REE pattern that is enriched relative the rest of the sample suite (**Figure 4a**). The clinopyroxene appears to be breaking down into fine grain olivine and amphibole during hydrothermal alteration, indicating that the clinopyroxene was melt-derived. The small amount of available material for sample KNR180-2 28-9 prohibited petrographic study, but it appears that both samples contain similar amphibole, clinopyroxene, plagioclase, and altered olivine. Both samples released over 90% of

their He during the 1600°C furnace step and showed $^3\text{He}/^4\text{He}$ ratios of $7.9 \pm 0.4 R_A$ (14-18) and $7.6 \pm 0.2 R_A$ (28-9), consistent with an upper mantle origin.

A gabbro-norite vein contained within a mylonitic harzburgite host (JAS113-59b(3)) displayed a large degree of variability when crushed twice ($2.7 \pm 0.2 R_A$ and $7.2 \pm 0.6 R_A$), and with low concentrations of He (1.6-2.1 ncc STP/g). The $2.7 R_A$ result was for a sampled core that was baked overnight at 100°C in an attempt to drive off excess H_2O . This sample therefore displayed a lower $^3\text{He}/^4\text{He}$ value, similar to other samples which were analyzed after baking. The variability may be indicative of sample heterogeneity and the varying addition of radiogenic and seawater helium components, or of isotopic fractionation induced by the baking procedure. When step heated this gabbro-norite vein released the majority of its He at 600°C, with a low $^3\text{He}/^4\text{He}$ ($3.1 \pm 0.3 R_A$ total), also consistent with an increased proportion of radiogenic helium (**Figure 3c**). The sample contained the highest U content in this study (0.14 ± 0.05 ppm), further providing support for a radiogenic imprint for the lower $^3\text{He}/^4\text{He}$ values (**Table 3**).

4.5 Evolved gabbro:

Two evolved, oxide gabbros were also analyzed (JAS 113-20 and KNR 180-2 5-30). Sample JAS113-20 released low concentrations of helium (0.95 ncc STP/g) for whole rock with a low $^3\text{He}/^4\text{He}$ ratio ($3.8 \pm 0.4 R_A$). The clinopyroxene mineral separate and the single step whole rock fusion analysis (1400°C) were below detection limit. A step heated extraction with a 1600°C step was not performed for these samples. The reason for the low He concentration is unknown, but it is possible the sample will react similarly to KNR180-2 14-18 and KNR180-2 28-9 wherein it releases the majority of its helium at 1600°C.

Sample KNR180-2 5-30 is an mylonitized oxide gabbro consisting of a deformed matrix of plagioclase containing amphibole and coarse grained (1-2 cm), partially serpentinized clinopyroxene. This sample is more complicated in that both the clinopyroxene and amphibole represent a magmatic origin but contain vastly different concentrations of REEs and He (**Figure 3b, 4**). The Nb concentration for the amphibole in 5-30 is 23.3 ± 2.3 ppm and the Nb/La ratio is 0.97 (consistent with magmatic range 0.8-20) as opposed to the ratio of 0.1 for KNR 180-2 14-18 (consistent with the hydrothermal range of 0.001-0.5 from *Coogan et al. (2001)*). The REE patterns show an enrichment in all REE, coupled with a negative Eu anomaly for the amphibole, while the clinopyroxene shows a depleted pattern (**Figure 4c**). The $^3\text{He}/^4\text{He}$ ranges from $7.9 \pm 0.3 R_A$ (crushed amphibole separate) to $1.45 \pm 0.2 R_A$ (whole rock total fusion). The amphibole in this sample was the most gas-rich mineral analyzed in this study. About 25% of the He in this amphibole was released by crushing, and its melted total $[\text{He}] = 115$ ncc STP/g. There is also significant isotopic disequilibrium within this amphibole. Crushing released helium having $^3\text{He}/^4\text{He} = 7.9 \pm 0.3 R_A$, while melting of whole grains of this mineral released helium having $4.3 \pm 0.3 R_A$. Radiogenic ingrowth has clearly affected the melted $^3\text{He}/^4\text{He}$, although the origin of the excess ^4He is unclear. The amphibole contained relatively low U concentrations of 0.007 ± 0.001 ppm, which would require up to 70 Myrs to produce the ^4He . There are no obvious apatite inclusions in thin section (see appendix) so it is hypothesized that a high U concentrated fluids or fine mineral deposits were incorporated along grain boundaries during hydrothermal alteration. The clinopyroxene in this same sample showed a small decrease in its isotopic ratio ($6.9 \pm 0.4 R_A$ to $6.1 \pm 0.3 R_A$) when crushed versus melted, but the low $[\text{He}]$ released by crushing makes it possible that some small amount of radiogenic helium may have led to reduced $^3\text{He}/^4\text{He}$.

compared to the initial ratio. The low $^3\text{He}/^4\text{He}$ for this whole rock sample ($1.5 \pm 0.2 R_A$) must result from a combination of mantle-derived, radiogenic and possibly seawater components.

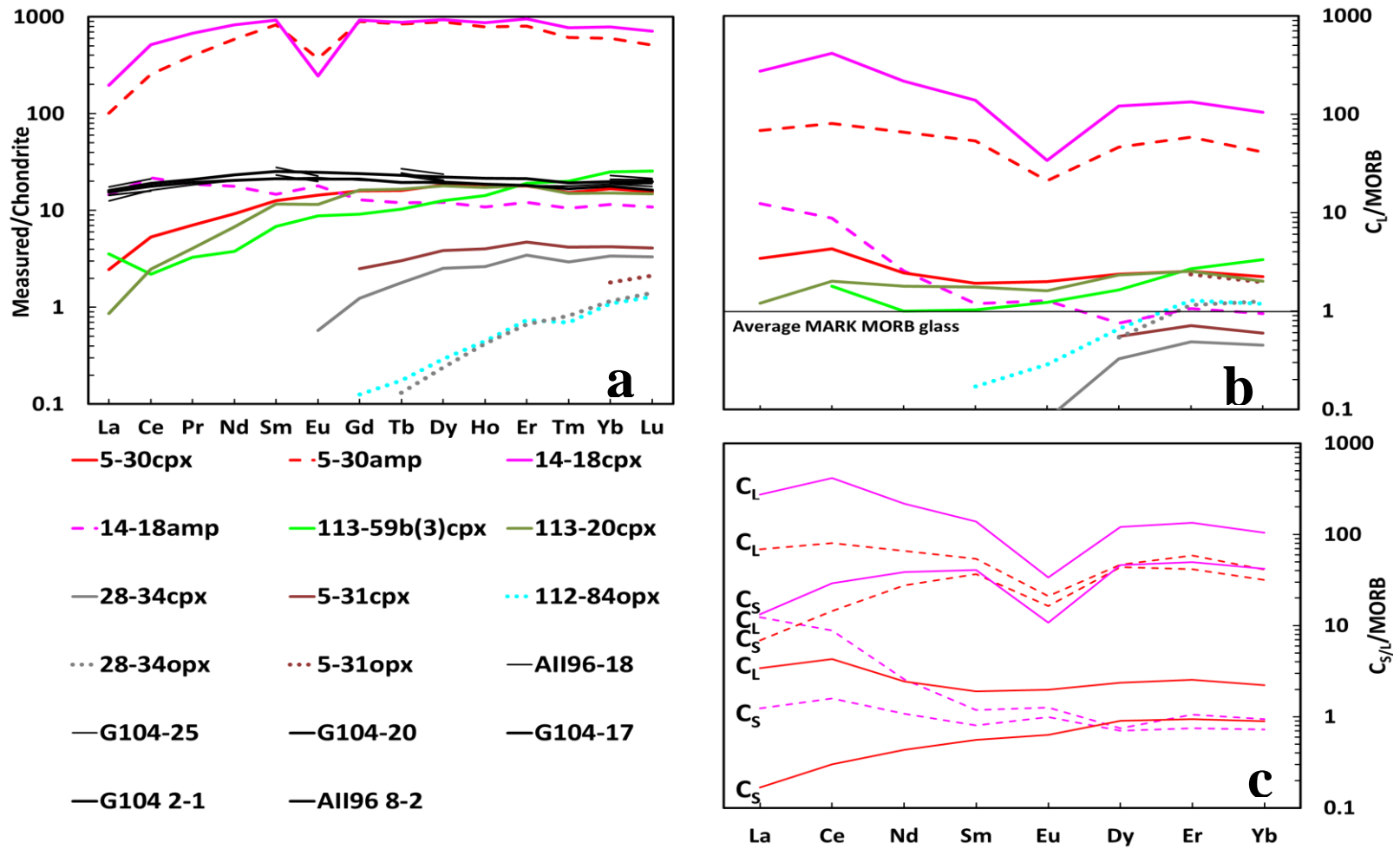


Figure 4: Color corresponds to sample location (as shown in fig. 1). Solid line: clinopyroxene, Dashed line: amphibole, Dotted line: orthopyroxene. A.) REE elements normalized to chondrite (*McDonough and Sun 1995*). B.) Calculated concentration in liquid (assuming the equation $D = C_{liq}/C_{solid}$) normalized to the average of the MORBs in (a). D_{cpx} values from *Johnson (1998)*, D_{opx} values from *McKenzie and O'Nions (1991)*, D_{amp} from *Tiepolo et al. (2007)*. C.) Calculated liquid (C_L) and measured solid concentrations (C_S) from amphibole and clinopyroxene in samples KNR180-2 14-18 and KNR180-2 5-30. Concentrations normalized to local MORB.

4.6 Carbon Dioxide from crushed peridotite and gabbro:

The CO₂ contents show considerable variability, and much of the observed variation appears to be a function of baking of the samples. **Figure 5** shows that CO₂ concentrations decrease significantly in samples that were baked at either 100°C or 50°C compared to when the same sample was not baked. Therefore, in most of the samples and especially in the mylonitized peridotites it seems that much of the CO₂ may be trapped loosely, perhaps in defects and along grain boundaries. Thus, even in samples which were not baked, it is difficult to resolve CO₂ in fluid/melt inclusions from that possibly added during interaction of the rocks with seawater and/or hydrothermal fluids.

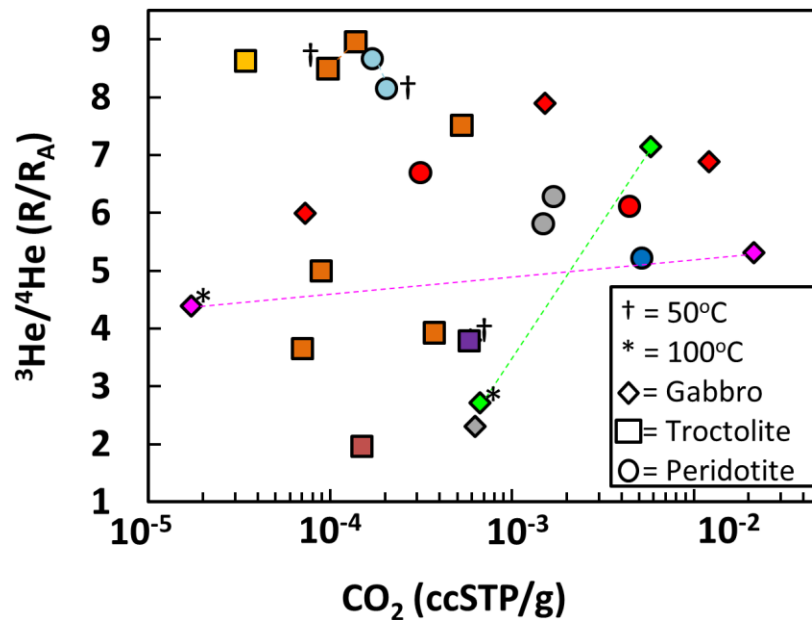


Figure 5: The CO₂ concentrations measured during crushing analysis versus the ³He/⁴He ratio. Samples below 10⁻⁴ cc STP/g are considered suspect due to the uncertainty in measuring CO₂ pressure at that level. Tie lines connect samples run as baked and unbaked and color represents sample location (as shown in figure 1).

5 DISCUSSION

5.1 Helium isotopic structure of the oceanic lithosphere at the Kane OCC

5.1.1 *Adam Dome:*

Five troctolites, one olivine gabbro vein, and one oxidized harzburgite were analyzed from Adam Dome (**Table 1**). This area consists of a large dunite body feeding a late stage troctolite intrusion ([Dick et al. 2008](#)). The troctolites analyzed in this area show a narrow range of $^3\text{He}/^4\text{He}$, between 8.6 and 9.0 R_A , similar to the range for the most depleted MORBs in the Atlantic (8.6 – 8.9 R_A ; [Graham et al. 1992](#)). They contain variable He concentrations which appear to depend on the degree of alteration and the sample's proximity to gabbroic veining. $^3\text{He}/^4\text{He}$ ratios of these rocks indicate that melt was sourced from a depleted mantle reservoir containing slightly elevated $^3\text{He}/^4\text{He}$ relative to the median value for MORB mantle (8.0-8.2 R_A ; [Graham 2002](#)). With the exception of the highly serpentinized sample KNR180-2 21-12, the troctolites are fresh and contain either trapped interstitial melt (in the form of high Mg# clinopyroxene) or are proximal to gabbroic veins (see [Lissenberg and Dick 2008](#) for more details). The troctolite samples containing gabbroic veins (JAS117-62, -63) were sampled within a few centimeters of those veins, and they contain only small amounts of helium (~4 ncc STP/g) that was effectively all released at the highest temperature step of 1600°C. Although the [He] of these samples is low, the measured $^3\text{He}/^4\text{He}$ is $8.8 \pm 0.4 R_A$, and within uncertainty for what was measured in the rest of the troctolite body. The gabbroic veins contain primarily clinopyroxene and plagioclase and show no measurable He when crushed or melted. The lack of He in the gabbroic veins and the reduced [He] in the surrounding troctolite suggest that He was mobilized from the crustal wall-rocks and removed into melt that was mobilized and transported away from the local environment now sampled by those rocks. The samples which contained trapped interstitial melt (JAS 117-61 and KNR 180-2 25-1) have the highest concentrations of helium in

the intrusive rocks of this study (up to 214 ncc STP/g). The relatively high [He] in these rocks has depleted mantle $^3\text{He}/^4\text{He}$ ratios of 8.8-9.0 R_A .

The gabbroic vein in the plagioclase peridotite (KNR 180-2, 28-9) analyzed from Adam Dome contained no measureable He when crushed, but a significant amount of He was released upon melting (64 ncc STP/g). When step heated, this sample released helium having $^3\text{He}/^4\text{He} = 4.5 \pm 0.4 R_A$ at the 1100°C step and $7.6 \pm 0.2 R_A$ at the 1600°C step. The increase in $^3\text{He}/^4\text{He}$ during step heating likely represents the release of an increased proportion of radiogenic ^4He during the 1100°C step, and the 1600°C step is therefore more likely to be representative of the initial $^3\text{He}/^4\text{He}$ of the rock. The $^3\text{He}/^4\text{He}$ of $7.6 R_A$ in this vein may represent either a conduit from a different, earlier mantle source feeding more enriched MORBs on the ridge (which we have neither found nor analyzed), or a greater degree of radiogenic contamination than what is seen in other Adam Dome troctolites. The harzburgite sample KNR180-2 28-34 also contained lower $^3\text{He}/^4\text{He}$, $\sim 6.3 \pm 0.5 R_A$ when crushed, and even lower values when melted.

One possibility is that rocks from Adam Dome other than the troctolites represent earlier formed melts from a lithologically heterogeneous mantle, while the late stage troctolites represent later stage melts from an ascending mantle ‘melt column’. The earlier formed melts appear to be characterized by slightly lower $^3\text{He}/^4\text{He}$ ratios of $\sim 7.5 R_A$ compared to the late stage melts, which gave rise to the large primitive gabbroic body having $^3\text{He}/^4\text{He}$ of ~ 8.7 -9.0 R_A . The later episode of melting may have tapped a more depleted mantle source (perhaps clinopyroxene-poor) in which a slightly less radiogenic helium signature is associated with a mantle lithology that was somewhat depleted in U and Th (e.g., harzburgite vs. lherzolite or garnet pyroxenite). Gabbroic veins which intruded the troctolite body at a somewhat later stage may have imparted a slightly elevated $^3\text{He}/^4\text{He}$, either injected laterally towards the MAR or when basalts were

erupted in an off-ridge volcanic field. Evidence of similar $^3\text{He}/^4\text{He}$ in the depleted MORBs (8.4-8.7 R_A) collected from the modern MAR near the Kane transform could indicate that they are also dominated by similar late stage melts.

5.1.2 *Cain and Abel Domes:*

The remaining rocks from this study come from Cain Dome, Abel Dome, or the valley between them. This area of the Kane OCC represents more subdued vertical ascent of primary mantle melt, as evidenced by the lack of dunite dredged in the area (*Dick et al. 2008*). The basement rocks of the area consist of massive, porphyroclastic peridotite with veins of differentiated melts. The sample JAS 112-84 was the freshest representative of these peridotites and contained relatively clean olivine, orthopyroxene, and clinopyroxene. The rock contained high concentrations of He (up to 170 ncc STP/g) and had a $^3\text{He}/^4\text{He}$ value of $8.4 \pm 0.2 R_A$. When crushed this sample contained a depleted isotopic value of $8.7 \pm 0.1 R_A$ which is within the range of local MORBs analyzed in this study. It is important to note that the olivine in this sample appears to be recrystallized, see **appendix XXI** (*Dick et al. 2010*) and possibly inherited its $^3\text{He}/^4\text{He}$ signature during late-stage mantle refertilization. The ultramafic olivine websterite vein dredged in the valley near the submersible dive 112 contained a depleted $^3\text{He}/^4\text{He}$ value of $8.6 \pm 0.3 R_A$ (1400°C total fusion analysis). This rock is likely a cumulate that formed *in-situ* with upwelling mantle melt, and appears to be in chemical equilibrium with surrounding peridotite (*Dick et al. 2010*). The $^3\text{He}/^4\text{He}$ values in these two peridotites are within error of the late stage troctolites from Adam Dome and the MORBs from near the Kane Fracture Zone. The depleted signature combined with the recrystallized nature of the olivine leads to some confidence that this signature was incorporated in the mantle during a second phase of melt flow through the area.

The olivine gabbro KNR180-2 14-18 had a $^3\text{He}/^4\text{He}$ of $7.9 \pm 0.4 R_A$ at 1600°C , and amphibole from the deformed oxide gabbro KNR180-2 5-30 had a $^3\text{He}/^4\text{He}$ of $7.9 \pm 0.3 R_A$ when crushed. These results indicate that this area may have sourced MORBs characterized by $^3\text{He}/^4\text{He}$ value of $\sim 8.0 R_A$. The high concentrations of He seen in the amphibole from sample KNR180-2 5-30 likely resulted from the evolved nature of the melt. In order to obtain an igneous amphibole in a MOR basaltic melt, 95% crystallization must occur in order to concentrate the H_2O needed in the melt ([Burnham 1979](#)). Such a high degree of crystallization would concentrate the incompatible elements such as He and the REEs, by a factor of 100, into the last phases to form. This makes igneous amphiboles potentially excellent recorders of the $^3\text{He}/^4\text{He}$ evolutionary history of the plutonic oceanic crust. Furthermore, these two gabbroic samples provide further evidence for the existence of a previous melt with a $^3\text{He}/^4\text{He}$ value close to the global median MORB ($8.0\text{--}8.2 R_A$, [Graham 2002](#)).

The mylonites from this area contained lowered $^3\text{He}/^4\text{He}$ values ranging from $2.1 - 5.4 R_A$, and most likely do not represent a primary melt signature. These samples are discussed further below in section 5.4.

5.2 Melting history beneath the Kane OCC:

By combining the He isotopic data with field relations and petrologic constraints from [Dick et al. \(2008; 2010\)](#) it is possible to theorize on the melting history of the mantle beneath the Kane OCC. **Figure 6** outlines two stages in the evolutionary history of the melting regime. An earlier stage involves melting of a heterogeneous MORB mantle having a weighted average $^3\text{He}/^4\text{He}$ composition near $8 R_A$. The large porphyroclastic harzburgite body from Cain and Abel Domes may have been developed largely through melting of lherzolite and/or garnet pyroxenite,

which produced some gabbroic intrusions within the mantle. The lack of dunite in this area of the OCC indicates that there was little to no vertical melt transport; the gabbroic intrusion probably occurred mainly as laterally injected veins originating to the east of Cain Dome ([Canales et al. 2008](#)). Although such a gabbroic body was not directly sampled in this study it seems likely that it would also be characterized by $^3\text{He}/^4\text{He}$ near 8.0 R_A . Melting of peridotite beneath the Adam Dome region also created veins of gabbro having lower $^3\text{He}/^4\text{He}$, near 7.5 R_A , although the potential small amounts of radiogenic ingrowth in our samples from this area also makes it possible that these melts initially carried a signature near 8 R_A . The exhumation of the lower crust and upper mantle during detachment faulting has affected all the samples in this study to some degree, and in the case of the peridotites it is likely to be responsible for the moderate to large degree of serpentinization, and the accompanying deformation marked by a notable grain size reduction in numerous places. If this shearing occurred primarily in the crust, significant helium loss may have occurred along with contamination by assimilation of a seawater-derived component.

A later stage of melting (either beneath the ridge or at some small distance away from the ridge axis), appears to have generated other magmas beneath Adam Dome, producing a large zone of dunite which fed large bodies of troctolite near the crust-mantle boundary. These troctolitic bodies contain a higher $^3\text{He}/^4\text{He}$ ratio of 8.7-9.0 R_A . These higher ratios in this later stage of melting may have resulted from preferential removal of more fusible (and slightly more ^4He -rich) lithologies, such as clinopyroxene, during the earlier melting stage. In some of these areas, however, the trapped melt still contains a relatively high concentration of He, so the earlier melting stage must not have extensively depleted the mantle source of its initial helium. Later melts flowing through such a troctolite host, evidenced by the late-stage gabbroic veins (which

seem to have stripped this slightly elevated $^3\text{He}/^4\text{He}$ signature from the host rock), may have transported much of the helium and other volatiles out of the veined troctolites. The observation that depleted basalts sampled from the adjacent ridge axis also have $^3\text{He}/^4\text{He}$ ratios of 8.4- 8.7 R_A suggests that those basalts, primarily from near the ridge – transform intersection, may be more representative of magmas derived from this later stage of melting.

In summary, in this area of the Mid-Atlantic Ridge we observe much of the global MORB range of $^3\text{He}/^4\text{He}$ away from high- ^3He hotspots, with values ranging from ~ 7 to 9 R_A . The range observed in the Kane region appears to be explained, at least partly, by evolution of the partial melting process for a lithologically heterogeneous mantle, in which slightly higher $^3\text{He}/^4\text{He}$ ratios occur in melts that were generated at later stages in the melting history.

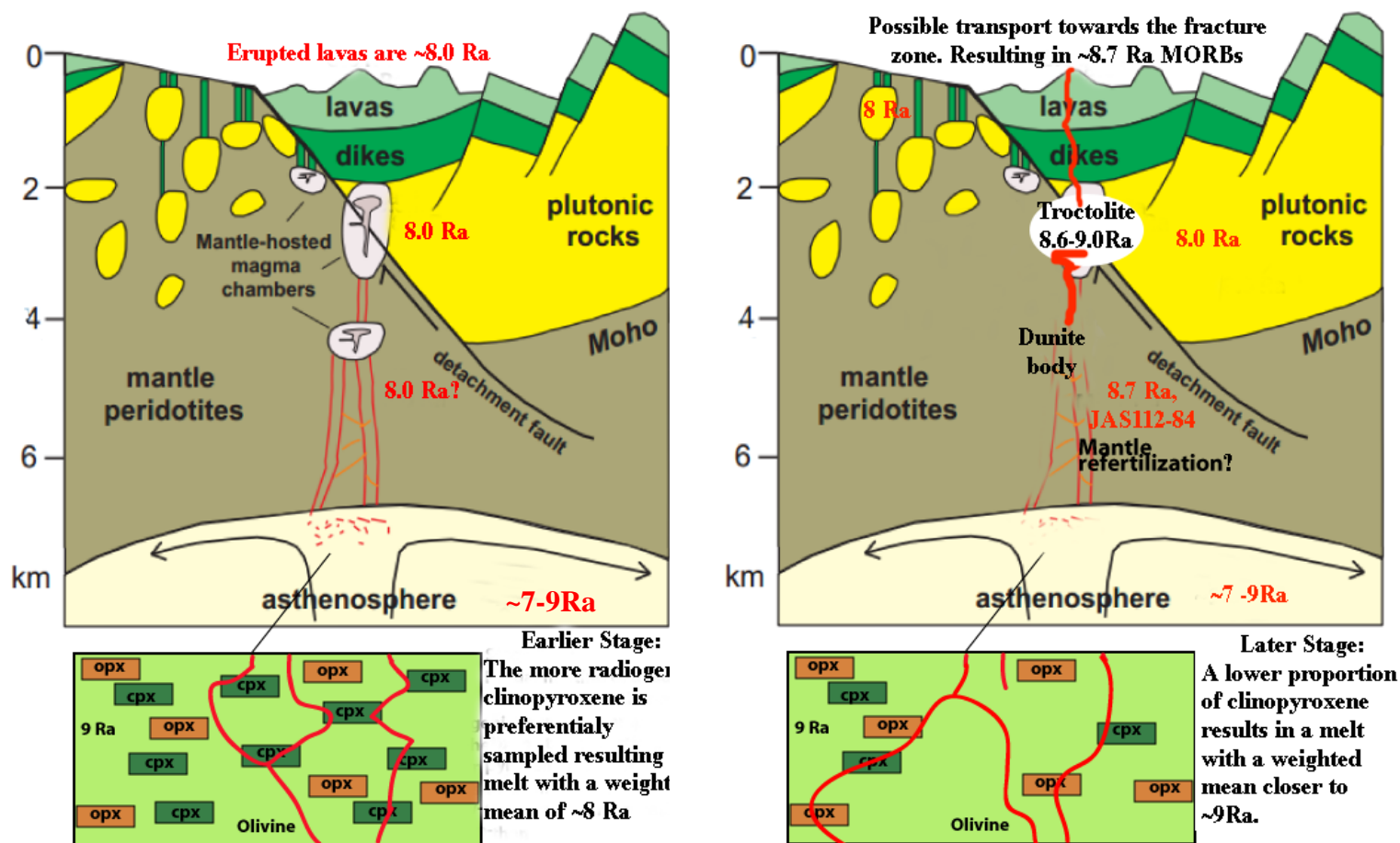


Figure 6: Schematic representation of two stages in the melting history beneath the Kane area on the MAR. Red lines schematically illustrate melt migration patterns. A.) Shows the earlier stage, with veins of melt feeding ridge volcanism having $^3\text{He}/^4\text{He}$ around the median MORB ratio ($8.0 R_A$). B.) Shows a later stage melt intrusion. This later stage melt taps a slightly elevated $^3\text{He}/^4\text{He}$ reservoir which is transferred into the crust (e.g., Adam Dome troctolites) and towards either the ridge near the fracture zone (e.g., depleted MORBs from this study). Sample JAS112-84 may have been either a result of melt refertilization of mantle peridotite or a residue of melting with very small amounts of trapped melt/fluid. Figure modified from [Pearce \(2002\)](#).

5.3 Melt-wallrock interaction and the representative nature of peridotite, gabbro and basalt

One of the goals of this study was to assess the potential effects of magma transport and melt-wallrock interaction on the helium isotope compositions of basalts erupted at the surface. To this aim, it is notable that the two peridotite samples Jas 112-84 (Harzburgite) and KNR 180-2 5-31 (olivine websterite) with relatively high helium contents yielded $^3\text{He}/^4\text{He}$ ratios of $8.6 \pm 0.2 R_A$, which is effectively identical to the range observed in the nine basalt glasses we also analyzed from the nearby Mid-Atlantic Ridge. The primitive troctolites with type 1 clinopyroxene, indicative of substantial trapped melt ([Lissenberg and Dick 2008](#)), also contain $^3\text{He}/^4\text{He}$ ratios within the range of the local depleted MORBs. These troctolites were considered to be representative of trapped interstitial melt with field relations showing they formed near the crust-mantle transition ([Dick et al. 2008](#)). The $^3\text{He}/^4\text{He}$ ratios in these rocks therefore show that the melt experienced little to no isotopic change during penetration and transport through the lower crust prior to being erupted on the seafloor. Although the peridotites, trapped melt in troctolites, and basalts have $^3\text{He}/^4\text{He}$ ratios within error of each other, gabbroic rocks from the same area have systematically lower $^3\text{He}/^4\text{He}$ ratios, even for samples with significant [He] (> 30 ncc STP/g). The gabbroic veins which appear to have formed somewhat earlier than the rocks at Adam Dome ([Dick et al. 2008](#)) may have fed a slightly more enriched section of the ridge. Work by [Bryan et al. \(1981\)](#), [Machado et al. \(1982\)](#) and [Reynolds and Langmuir \(1997\)](#) show that the MORBs along the Mid-Atlantic Ridge become more enriched as one moves southward from the Kane transform. Thus, a good future test will be to examine $^3\text{He}/^4\text{He}$ ratios in those basalts to see if they are similar to the gabbros in this study ($\sim 8 R_A$). It is also possible that the gabbros were

fed from a different mantle source than any basaltic counterpart. It is possible that a veined peridotite or enriched blob of pyroxenite in the mantle contributed melt for the gabbros, with a more radiogenic He isotope signature, due to the typically higher contents of U in pyroxenite (~20-90 ppb) compared to peridotite (~10-20 ppb) (e.g., [Stracke et al. 2009](#)). In this case, however, it is difficult to account for the absence of basalt with the same enriched signature, given that these types of mantle lithologies are more fertile, and produce more melt per km of ascent, than peridotite.

5.4 Role of shearing, alteration and metamorphism of peridotite

In contrast to [Kurz et al. \(2009\)](#) we did not observe a good relationship between the He concentration of ultramafic rocks from the Kane OCC and their extent of deformation. In fact, the highest He concentrations occur in the freshest and least deformed peridotites. **Figure 7** shows the relationship between shearing and grain deformation (using the grades described in [Dick et al. 2008](#) and [Kurz et al. \(2009\)](#)); wherein increasing numbers reflect an increasing degree of deformation.

It seems likely that the mylonitic rocks of this study are not truly representative of the role of shearing in the uppermost mantle, but instead record stages of shearing during exhumation on the seafloor. Sample JAS 113-59 contains a zone of talcose-chloride representing the fault wall onto which it was exhumed. Therefore it is likely that the bulk of the shearing and deformation in these particular samples relate to crustal exhumation. This makes them unlikely to have incorporated mantle He during the deformation, but potentially to have been influenced by incorporation of some small amounts of helium derived from seawater. The coupling of grain size reduction with serpentinization in fluids at ~500°C may degas the total [He] from the sample

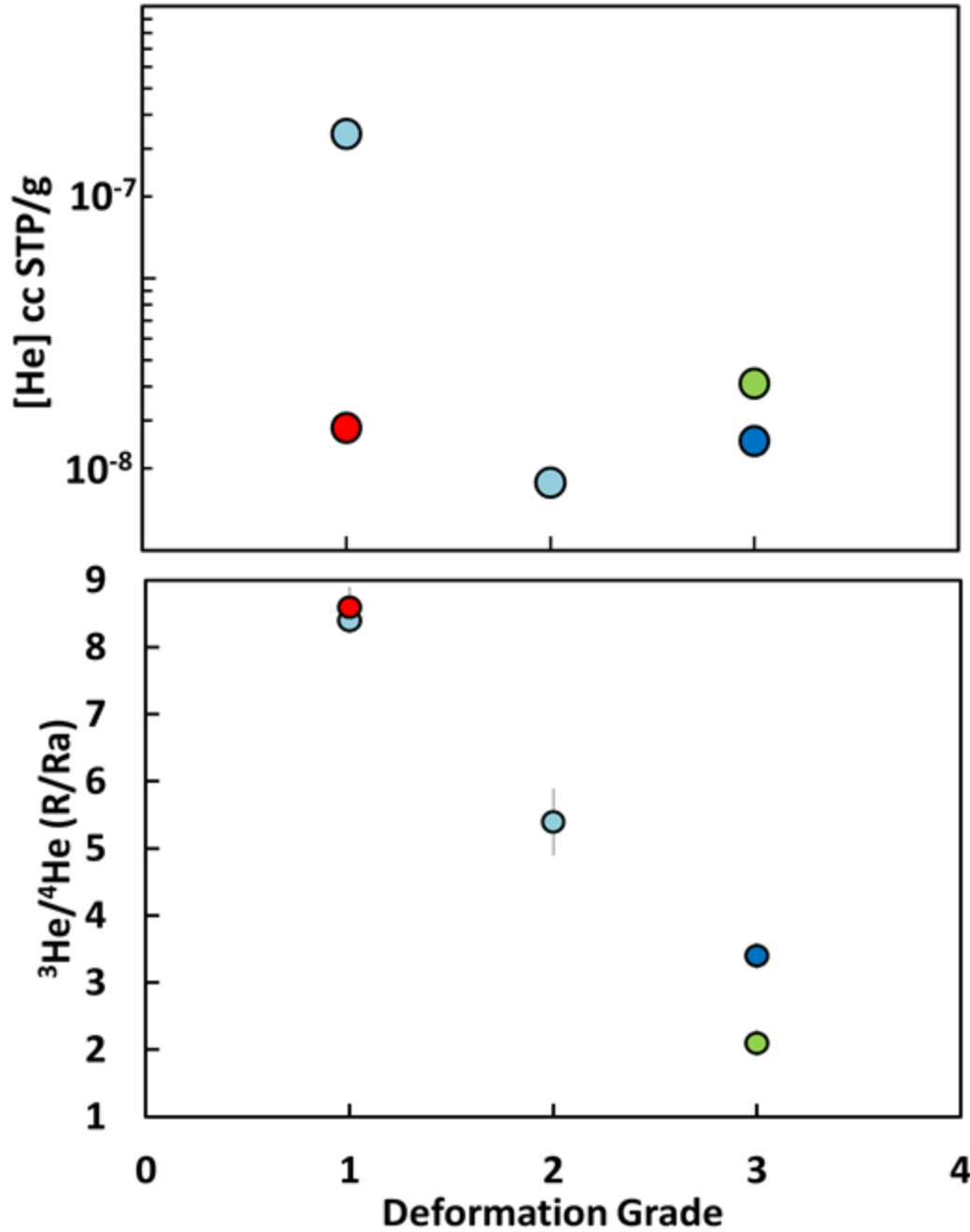


Figure 7: Deformation grade (from [Kurz et al. 2009](#)) versus [He] and $^3\text{He}/^4\text{He}$ ratio measured from the total melted extraction. Color represents the location of the sample (figure 1). Error bars are $\pm 2\sigma$. The sample KNR180-2 5-31 (red circle) represents a minimum concentration due to an incomplete extraction at 1400°C.

and either isotopically fractionate ^3He from ^4He , incorporate a small concentration of He from seawater, or a combination of both.

5.5 Analyzing ocean lithospheric rocks

The study of helium isotopes in ocean plutonic rocks is a relatively young field. In order to better understand the most efficient means of analyzing lithospheric rocks for He geochemistry this study analyzed rocks through different means such as crushing, baking during preparation, step heating, and total fusion experiments.

5.5.1 Crushing:

Unlike the commonly analyzed MORB glass, crushing is generally not an efficient means of obtaining a reliable He measurement in plutonic rocks. With the exception of two troctolite samples, 70-100% of the ^3He was released during heating analysis (**Table 2**). Mylonitic peridotites contained the lowest ratio of crushed to melt [He] out of the sample set, typically releasing 0 – 5% of He during crushing analysis. Whether this is a function of the crushed samples being baked prior to analysis or if the fine grain nature of mylonite prevents efficient release of He during crushing was not determined in this study. [Kurz et al. \(2009\)](#) found only ~10% of He in mylonites was released during crushing and given the higher concentration of He released during total fusion in that study, our results don't significantly differ. The majority of helium in each lithology is located in either the inter-crystalline matrix, in small fluid inclusions (probably <5 μm in diameter), or along grain boundaries. In the samples JAS 112-84, KNR180-2 5-31, and KNR180-2 21-12 fluid inclusions are visible in olivine, most commonly occurring as parallel lines of opaque 'blobs' which run through the crystal (**Appendix Figure A1**). These are interpreted to represent trapping of fluid during annealing of stress fractures at high temperature ([Natland 2003](#)). We hypothesize that these small inclusions (<5 μm) are not efficiently sampled during crushing, since the resulting powder is almost entirely greater than 5 μm on average. The troctolites KNR180-2 25-1 and JAS117-61 contain course grained fresh olivines with larger fluid

inclusions, these samples contained the highest crushed/melt [He] ratio at 0.46-0.21, which appears to be indicative of a more efficient release of He when the inclusions are coarser.

Some samples were baked at 50°C and 100°C in order to better drive off high concentrations of H₂O prior to crushing extraction. When rocks were crushed after baking compared to analysis without baking there was a decrease in ⁴He concentration among the samples having higher He concentrations, while ³He/⁴He ratios decreased significantly (outside of the 95% confidence interval in every case) (**Figure 8**). It is important to note that sample heterogeneity may lead to some concentration and ³He/⁴He ratio variation, but the present results are relatively systematic in the direction of behavior. In summary, although high concentrations of H₂O and H may increase pressure in the extraction line there appears to be some loss of He combined with isotopic fractionation during baking.

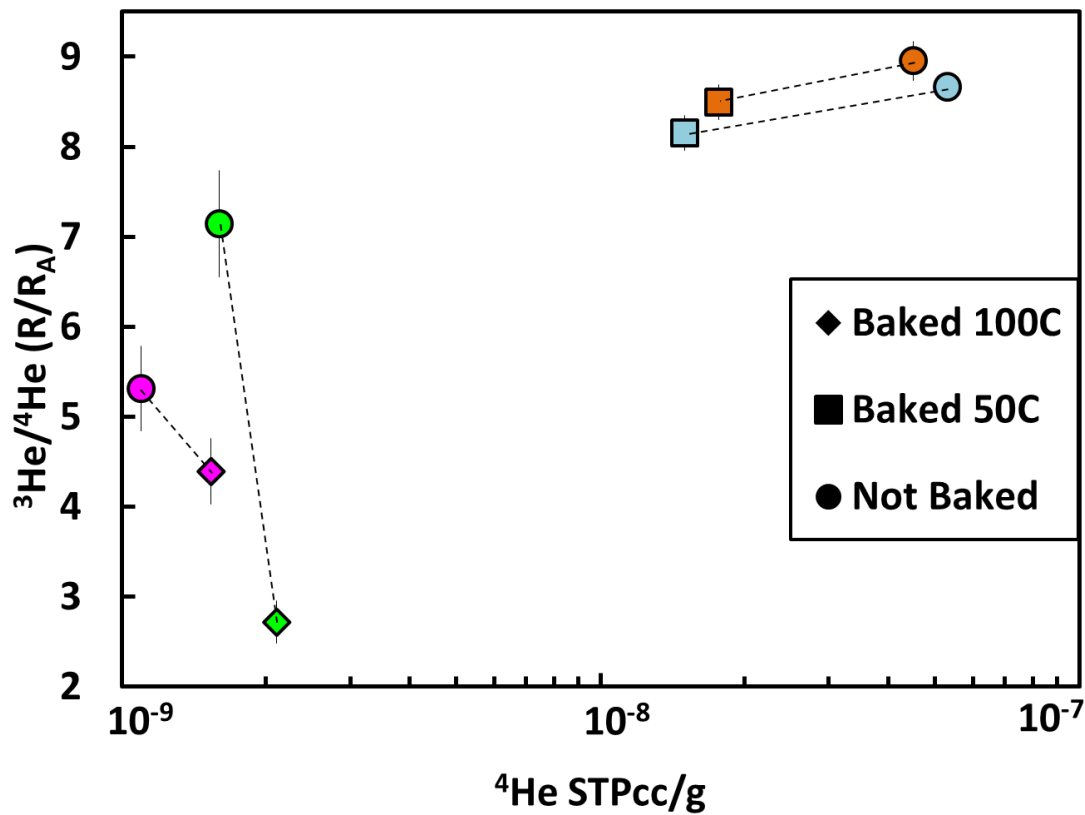


Figure 8: Crushed analyses of samples run with and without baking. Samples were baked between 16-18 hours under vacuum prior to analysis. Samples are KNR180-2 14-18 olivine gabbro (purple), JAS113-59b(3) gabbro-norite vein (green), JAS117-61 troctolite (orange), and JAS112-84 harzburgite (blue). Tie lines connect same sample.

5.5.2 *Melting analysis:*

Samples were initially analyzed by 1400°C total fusion experiments. Hot blanks run at 1450°C between samples were low, except after sample JAS112-84 which contained significant He levels. In the second batch of melting experiments when, the furnace was run at 1600°C significantly more He was released from the same analyzed samples, so the previous experiments were treated as a minimum concentration. Melting cores of rock instead of crushed powders required higher temperature steps at longer duration in order to quantitatively extract all He from the sample. All samples were re-analyzed at three temperature steps; 600°C, 1100°C, and 1600°C, held at peak temperature for 20 minute in each step. The results were much more informative than previous total fusion experiments, which were more strongly influenced by lowered $^3\text{He}/^4\text{He}$ ratios from alteration released at low temperature steps.

Due to the fine grained nature of fluid inclusions and the primary residence of He in crystal lattice sites and/or fine inclusions in these rocks, step heating followed by melting is the most informative means of analysis. For example, the heavily serpentinized troctolite KNR180-2 21-12 crushed analysis had 3 ncc STP/g of ^4He with a $^3\text{He}/^4\text{He}$ ratio of $3.8 \pm 0.3 R_A$. During step heating analysis ~3 ncc STP/g of ^4He was released during the 600°C and 1100°C steps combined with ~6.7 R_A . The remaining 12 ncc STP/g of ^4He released at the 1600°C temperature step had a ratio of $8.8 \pm 0.4 R_A$. The ratio of 8.8 R_A is within the range of troctolites in the same region (8.6-9.0 R_A) and thus the total fusion ratio of 8.4 R_A is somewhat lower than the value representative of the primary signature of the rock.

Powders of crushed samples were not melted in this study due to the large time gap between many of the crushing and melting analysis (~1 year), which makes helium loss by diffusion a potential problem. With the majority of He in these samples being released during melting extractions, the most efficient means of analysis would be crushing followed by at least two steps of heating the powders, and subsequent total fusion.

6 SUMMARY

The Kane OCC represents the full spectrum of oceanic lithospheric rocks and $^3\text{He}/^4\text{He}$ ratios seen in MORBs around the globe. After accounting for radiogenic, seawater, and degassing related alteration four main conclusions arrive:

1. There appears to be two separate melting stages beneath the Kane region. An early enriched melt stage having a $^3\text{He}/^4\text{He}$ value of $\sim 7.7\text{-}8.0 R_A$, as recorded in some gabbros. This was followed by a late-stage depleted melt having a $^3\text{He}/^4\text{He}$ value of $8.6\text{-}9.0 R_A$, as recorded in fresh peridotite, troctolite, and MORBs from near the Kane transform.
2. The MORB glasses appear to be in isotopic equilibrium with both fresh peridotite and troctolite from the Kane OCC. The troctolite represents a late stage depleted melt intrusion emplaced near the MOHO and thus indicates that there is little to no fractionation of $^3\text{He}/^4\text{He}$ from penetration into the crust to eruption on the seafloor. A lower $^3\text{He}/^4\text{He}$ ratio, similar to the gabbros has not yet been measured in Kane MORBs. MORBs further down the MAR from the Kane fracture zone show increased trace element enrichment ([Bryan et al. 1981](#)) and may be more representative of the early melt signature.
3. Mylonites from the Kane OCC show a decrease in He concentration and $^3\text{He}/^4\text{He}$ relative to fresh peridotites. The decrease may be a factor of degassing during exhumation

followed by radiogenic ingrowth, introduction of small amounts of helium from seawater, and/or fractional degassing.

4. Due to the degree of alteration and the low concentrations of He released during crushing, the most efficient means of analyzing lithospheric rocks is crushing, followed by step heating extractions of the powders. Baking lithospheric samples in order to drive off excess H₂O appears to fractionate the $^3\text{He}/^4\text{He}$ value and distorts the CO₂ concentrations.

7 REFERENCES

- Asimow, P. 1999. A model that reconciles major- and trace-element data from abyssal peridotites. *Earth and Planetary Science Letters*. 169. 303-319
- Brandon, A.D., Snow, J.E., Walker, R.J., Morgan, J.W., Mock, T.D. 2000. ^{190}Pt - ^{186}Os and ^{187}Re - ^{187}Os systematics of abyssal peridotites. *Earth and Planetary Science Letters*. 177, 319-335
- Bryan, W. B., Thompson, G., and Ludden, J. N., 1981. Compositional variation in normal MORB from 22° -25°N: Mid-Atlantic Ridge and Kane Fracture Zone. *J. Geophys. Res.* 86, 11815-11836.
- Burnham, C.W. 1979. Magma and hydrothermal fluids. In Barnes, H.L., (Ed.) *Geochemistry of Hydrothermal Ore Deposits*: New York (Wiley), 71-133
- Canales, J.P., Tucholke, B., Xu, B.E., Collins, J.A and DuBois, D.L., 2008. Seismic evidence for large scale compositional heterogeneity of oceanic core complexes. *Geochemistry, Geophysics, Geosystems*, 9
- Cipriani, A., Brueckner, H., Bonatti, E., and Brunelli, D., 2004. Oceanic crust generated by elusive parents: Sr and Nd isotopes in basalt-peridotite pairs from the Mid-Atlantic Ridge. *Geology* 32, 657-660.
- Constantin, M., Hekinian, R., Bideau, D., Hebert, R. 1996. Construction of the oceanic lithosphere by magmatic intrusions: Petrological evidence from plutonic rocks from along the fast-spreading East Pacific Rise. *Geology*. 24. 731-734
- Coogan, L.A., Wilson, R.N., Gillis, K.M., MacLeod, C.J. 2001. Near-solidus evolution of oceanic gabbros: Insights from amphibole geochemistry. *Geochimica et Cosmochimica Acta*. 65. 4339-4357
- Dick, H. J. B., Natland, J. H., and Ildefonse, B., 2006. Past and future impact of deep drilling in the oceanic crust and mantle. *Oceanography* 19, 72-80.
- Dick, H. J. B., Tivey, M. A., and Tucholke, B. E., 2008. Plutonic foundation of a slowspreading ridge segment: oceanic core complex at Kane Megamullion, 23°30'N, 45°20'W *Geochemistry, Geophysics, Geosystems*. 9, doi:10.1029/2007GC001645.
- Dick, H.J.B., Lissenberg, J.C., and Warren, J.M., 2010. Mantle Melting, Melt Transport, and Delivery Beneath a Slow-Spreading Ridge: The Paleo-MAR from 23°15'N to 23°45'N. *Journal of Petrology*. 51 (1&2), 425-467
- Elthon, D. 1992. Chemical Trends in Abyssal Peridotites: Refertilization of Depleted Suboceanic Mantle. *Journal of Geophysical Research*. 97. 9015-9025.
- Farley, K.A., and Neroda, E. 1998. Noble Gases in the Earth's mantle. *Annu. Rev. Earth Planet. Sci.* 26, 189-218
- Faul, U.H. 2001. Melt retention and segregation beneath mid-ocean ridges. *Nature*. 410. 920-923
- Graham, D.W., Jenkins, W.J., Schilling, J.G., Thompson, G., Kurz, M.D., Humpris, S.E. 1992. Helium isotope geochemistry of mid-ocean ridge basalts from the South Atlantic. *Earth and Planetary Science Letters*. 110. 133-147

- Graham, D. W., 2002. Noble gas isotope geochemistry of mid-ocean ridge and ocean island basalts; characterization of mantle source reservoirs. In: Porcelli, D., Wieler, R., and Ballentine, C. J. Eds.), *Noble Gases in Geochemistry and Cosmochemistry*. Mineral. Soc. Amer, Washington, D.C.
- Harvey, J. Gannoun, A., Burton, K.W., Roger, N.W., Alard, O., Parkinson, I.J. 2006. Ancient melt extraction from the oceanic upper mantle revealed by Re-Os isotopes in abyssal peridotites from the Mid-Atlantic ridge. *Earth and Planetary Science Letters*. 244. 606-621
- Johnson, K.T.M., Dick, H.J.B., Shimizu, N. 1990. Melting in the oceanic upper mantle: an ion microprobe study of diopsides in abyssal peridotites. *Journal of Geophysical Research*. 95. 2661-2678
- Johnson, K.T.M. 1998. Experimental determination of partition coefficients for rare earth and high-field strength elements between clinopyroxene, garnet, and basaltic melt at high pressures. *Contributions to Mineralogy and Petrology*. 133. 60-68
- Katz, R.F., Weatherly, S.M. 2012. Consequences of mantle heterogeneity for melt extraction at mid-ocean ridges. *Earth and Planetary Science Letters*. 335-336. 226-237
- Kelemen, P.B., Koga, K., Shimizu, N. 1997. Geochemistry of gabbro sills in the crust-mantle transition zone of the Oman ophiolite: implications for the origin of oceanic lower crust. *Earth and Planetary Science Letters*. 146. 475-488
- Kumagai, H., Dick, H. J. B., and Kaneoka, I., 2003. Noble gas signatures of abyssal gabbros and peridotites at an Indian Ocean core complex. *Geochem. Geophys. Geosys.* 4, Paper 2003GC000540.
- Kurz, M.D. 1993. Mantle Heterogeneity beneath Oceanic Islands: Some Inferences from Isotopes. *Philosophical Transactions: Physical Sciences and Engineering*, 342, 91-103.
- Kurz, M. D., Warren, J.M., and Curtice, J., 2009. Mantle deformation and noble gases: Helium and neon in oceanic mylonites. *Chemical geology*. 266, 10-18
- Lissenberg, C. J. and Dick, H. J. B., 2008. Melt-rock reaction in the lower oceanic crust and its implications for the genesis of mid-ocean ridge basalt. *Earth Planet. Sci. Lett.* 271, 311-325.
- Lizarralde, D., Gaherty, J.B., Collins, J.A., Hirth, G., Kim, S.D. 2004. Spreading-rate dependence of melt extraction at mid-ocean ridges from mantle seismic refraction data. *Nature*. 432. 744-747.
- Lupton, J., Evans, L. 2004. The atmospheric helium isotope ratio: Is it changing? *Geophysical Research Letters*. 31. 1-5
- Machado, N., Ludden, J.N., Brooks, C., Thompson, G. 1982. Fine-scale isotopic heterogeneity in the sub-Atlantic mantle. *Nature*. 295. 226-228
- Macleod, C.J., Searle, R.C., Murton, B.J., Casey, J.F., Mallows, C., Unsworth, S.C., Achenbach, K.L., Harris, M. 2009. Life cycle of oceanic core complexes. *Earth and planetary Science Letters*. 287, 33-344.

- Marty, B., Jambon, A. 1987. C^3He in volatile fluxes from the solid Earth: implications for carbon geodynamics. *Earth and Planetary Science Letters*. 83. 16-26
- Marty, B., Zimmerman, L. 1999. Volatiles (He, C, N, Ar) in mid-ocean ridge basalts: assessment of shallow-level fractionation and characterization of source composition. *Geochimica et Cosmochimica Acta*. 63. 3619-3633
- Matsuda, J., Matsumoto, T., Sumino, H., Nagao, K., Yammaoto, J., Miura, Y., Kaneoka, I., Takahata, N., Sano, Y. 2002. The $^3He/^4He$ ratio of the new internal He Standard of Japan (HESJ). *Geochemical Journal*. 36. 191-195
- McDonough, W.F., Sun, S. 1995. The composition of the Earth. *Chemical Geology*. 120. 223-253
- McKenzie, D. O'Nions, M.K. 1991. Partial melt distributions from inversion of rare earth element concentrations. *Journal of Petrology*. 32. 1021-1091
- Meurer, W.P. Sturm, M.A. Klein, E.M. Karson, J.A. 2001. Basalt compositions from the Mid-Atlantic Ridge at the SMARK area (22°30'N to 22°50'N)- implications for parental liquid variability at isotopically homogeneous spreading centers. *Earth and Planetary Science Letters*. 186. 451-469
- Moreira, M., Blusztajn, J., Curtice, J., Hart, S. R., Dick, H. J. B., and Kurz, M. D., 2003. He and Ne isotopes in oceanic crust: implications for noble gas recycling in the mantle. *Earth Planet Sci. Lett.* 216.
- Morris, E., Detrick R.S., 1991. Three-dimensional analysis of gravity anomalies in the MARK area. Mid Atlantic Ridge 23°N. *Journal of Geophysical Research*. 96, 4355-4366.
- Natland, J.H. 2003. Capture of helium and other volatiles during the growth of olivine phenocrysts in picritic basalts from the Juan Fernandez islands. *Journal of Petrology*. 44. 421-456
- Ozima, M., and Podosek, F.A. 1983. Noble Gas Geochemistry, *Cambridge University Press*, Ny, 367pp.
- Pearce, J. 2002. The Oceanic Lithosphere. *The JOIDES Journal*. 28. 62-66
- Porcelli, D. and Elliott, T., 2008. The evolution of helium isotopes in the upper mantle and the generation of isotopic anomalies. *Earth and Planetary Science Letters*. 269, 175-185.
- Reynolds, J. R. and Langmuir, C. H., 1997. Petrological systematics of the Mid-Atlantic Ridge south of Kane: implications for ocean crust evolution. *Journal of Geophysical Research*. 102, 14915- 14946.
- Salters, V. J. M. and Dick, H. J. B., 2002. Mineralogy of the mid-ocean-ridge basalt source from neodymium isotopic composition of abyssal peridotites. *Nature* 418, 68-72.
- Seyler, M., Toplis, M.J., Lorand, J.P., Luguët, L., Cannat, M. 2001. Clinopyroxene microtextures reveal incompletely extracted melts in abyssal peridotites. *Geology*. 29. 155-158
- Seyler, M., Lorand, J.P., Toplis, M.J., Godard, G. 2004. Asthenospheric metasomatism beneath the mid-ocean ridge: Evidence from depleted abyssal peridotites. *Geology*. 32. 301-304.

- Staudacher, T. Sarda, P., Richardson, S.H., Allegre, C.J., Sagna, I., Dmitriev, L.V. 1989. Noble gases in basalt glasses from a Mid-Atlantic Ridge topographic high at 14°N: geodynamic consequences. *Earth and Planetary Science Letters*. 96, 119-133.
- Stracke, A., Bourdon, B. 2009. The importance of melt extraction for tracing mantle heterogeneity. *Geochimica et Cosmochimica Acta*. 73. 218-238
- Tivey, M. Tucholke, B., Dick, H., 2004. Kane Megamullion 2004, cruise report KN180-2, Woods Hole Oceanographic Institution. 53pp
- Tourmey, D.R., Grove, T.L, Bryan, W.B. 1987. Experimental petrology of normal MORB near the Kane Fracture Zone: 22°-25°N, mid-Atlantic ridge. *Contributions to Mineralogy and Petrology*. 96. 121-139
- Williams, C. M. 2007. Oceanic Lithosphere magnetization: Marine magnetic investigation of crustal accretion and tectonic processes in Mid-ocean ridge environments, Cambridge, MA: Massachusetts Institute of Technology; Woods Hole, MA: Woods Hole Oceanographic Institution, 285 pp.

KNR180-2 14-18

Lithology: Olivine Gabbro with an amphibolite facies plagioclase vein

Location: 23.461N, 45.306W. Dredge 14, Cain Dome.

Analysis: Helium, Electron Microprobe, LA-ICPMS

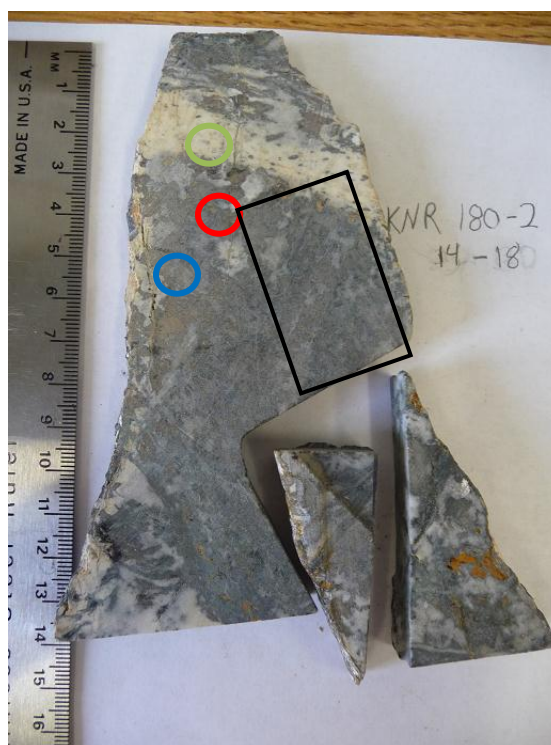
Image of KNR180-2 14-18 (right) prior to sampling.

Circles represent the location of drilled cores:
Red: KNR180-2 14-18(1)a* & b(½ core baked and ½ not baked)

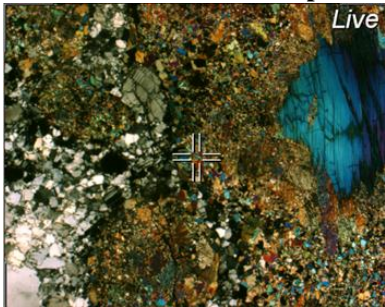
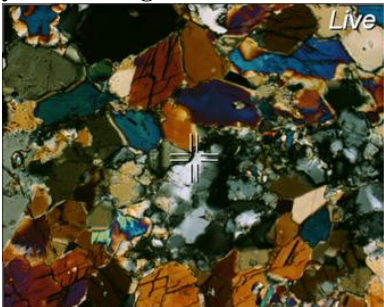
Blue: KNR180-2 14-18(1) (melted)

Green: KNR180-2 14-18(2)*

Thin section location is roughly outline by the black rectangle.



Comments: The whole rock crushing analysis was repeated after concerns about the effects of baking samples were raised. Following the trend of other samples which were analysed with and without baking the baked sample contained a lower $^3\text{He}/^4\text{He}$ ratio than the non-baked sample. The overall concentration of the non-baked sample (1.1 ncc/g) was lower than the baked sample (1.5 ncc/g) but at the low concentrations of these measured samples it is considered a factor of heterogeneity in the sample and the role of baking is harder to determine. The plagioclase vein was never melted due to a mal-function of the furnace prior to analysis.

Sample		KNR 180-2 14-18		
Rock Name		Olivine Gabbro		
Hand Sample Description:				
A large cut rock section with a ~2 cm plagioclase rich vein cutting a gabbroic section. Appears to have some degree of metamorphic deformation. Alteration products seen only on the edges of the hand sample.				
Microscopic Description				
Vol%	Mineral	Size (mm)	Shape	Distinguishing Features
	CPX	up to 3cm	Subhedral	
	Amphibole	<0.25	sub-euhedral	Occur in patches clumped together, 120 degree cleavage. Brown pleochroism
	Plagioclase	250um-6mm	anhedral	Deformation patterns of fine grained plag with course grained plag scattered throughout
	Olivine	0.25	an-euhedral	occur around CPX
Textual Features, Alteration, Deformation Grade, ect				
Occurs in three sections. There are deformation bands of plagioclase with course <6mm plagioclase throughout the entire sample. There are course cpx crystals surrounded by olivines and alteration products. It appears that the cpx is breaking down during some high temperature alteration event. Lastly there are bands of amphibole which are really clean filling shear zones.				
<div style="display: flex; justify-content: space-around;">   </div>				
Photos:				
	Whole Rock	Amphibole		
Field of View	11mm	2.5mm		

KNR180-2 5-30

Lithology: Oxide Gabbro
Mylonite

Location: 23.471N, 45.358W.
Cain Dome.

Analysis: Helium, Electron
Microprobe, LA-ICPMS
Image of KNR180-2 5-30 (right)
prior to sampling.

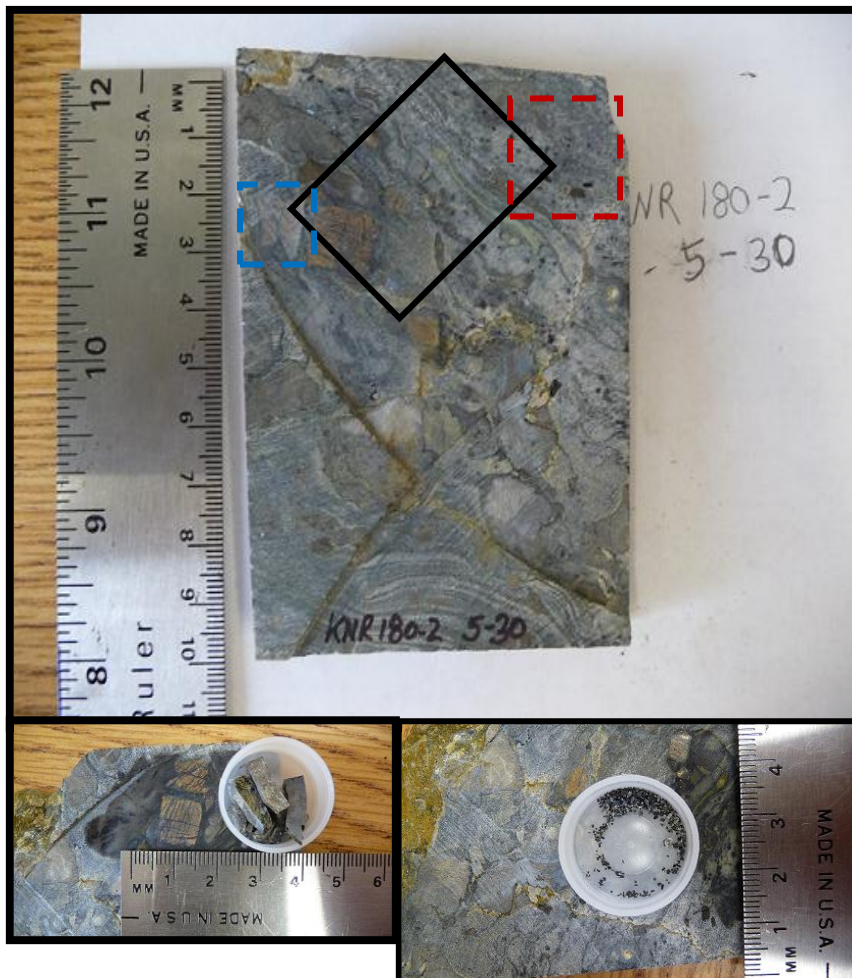
Dash red square is the location
where WR chips were taken and
where amphibole was separated
(Bottom right).

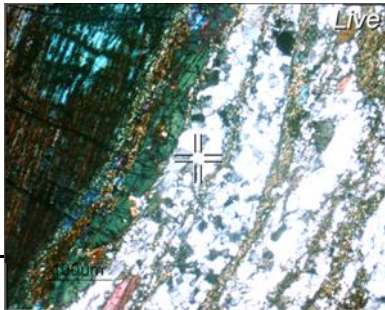
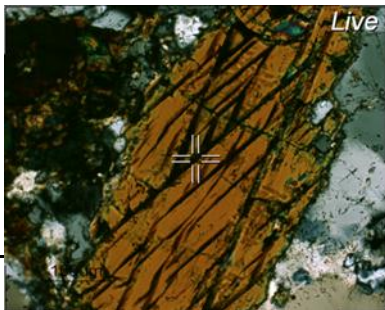
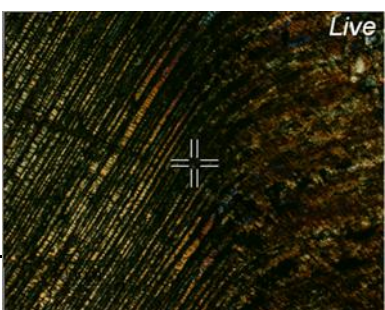
Blue dashed square is where the
clinopyroxene separate was taken.
The same grain (~2cm) was used
for crushing, melting, some probe
data, and LA-ICPMS analysis
(Bottom left).

Black rectangle is the rough
location where the thin section
was made.

Comments: The clinopyroxene
separate contained upwards of
10% black serpentine alteration
filling gaps between crystal faces.

Amphibole separates consisted of
upwards of 5% plagioclase clinging to the crystal surface. Bands of deformation are clear in hand
sample and amphibole appears to run along them with bands of greenish alteration filling shear
zones. The whole rock chips consisted of plagioclase, amphibole, and alteration in the deformed
shear zone. Clinopyroxene was not included in whole rock analysis. Microprobe analysis was
taken both of minerals in thin section and minerals left over from crushing analysis. LA-ICPMS
work was done on mineral separates.



Sample		KNR 180-2 5-30		
Rock Name		Oxide Gabbro Mylonite		
Hand Sample Description:				
Course (1-3cm) CPX aggregates in a matrix of deformed plagioclase and amphibole. Pockets of green alteration appear along deformation bands. CPX is brown/gold and amphibole is black in hand sample. Amphiboles clearly stand out among the plagioclase dominated matrix.				
Microscopic Description				
Vol%	Mineral	Size (mm)	Shape	Distinguishing Features
40	Clinopyroxene	100-300	subhedral	Shows some bent lamina which can be used as a thermometer
10	Amphibole	<1	subhedral	120o cleavage. Found both on the edges of course cpx crystals and floating in the plagioclase matrix
45	Plagioclase	0.25 - 0.5	anhedral	Found in a deformation matrix. Fairly homogenous grain size
5	orthopyroxene?	0.1	anhedral	Possibly some opx around the course cpx. Hard to tell.
Textual Features, Alteration, Deformation Grade, ect				
Cpx contains serpentized veins both along the lalleme and across the crystal. Some samples are significantly serpentized and show no birefringence. The lamelle occasionally display a bent nature (see below). The edges of the CPX are breaking down into amphibole and possibly olivine or opx which form fine grain rims. There is occasional alteration zones, although it is not well represented in this section. Amphiboles are found ranging in size from 250-1000um floating in the plagioclase matrix.				
<div><div><div>Live</div></div><div><div>Live</div></div><div><div>Live</div></div></div>				
whole rock shot		Amphibole		CPX
Field Of View	11mm	5.5mm		5.5mm

KNR180-2 28-9

Lithology: Olivine Gabbro Vein in harzburgite

Location: 23.383N, 45.382W. Adam Dome

Analysis: Helium

Image of KNR180-2 28-9 (right).

Red core = Crushed

Blue circle = Melted

Small cores were taken of each to avoid contamination from the harzburgite host. Harzburgite was not sampled. It is uncertain which blue core location represents the published step heating experiments.



Comments: Small vein of what appears to be amphibole and plagioclase bearing gabbro. Thin section analysis to determine the sample type was done by Henry Dick and the author has not seen the section. Microprobe data on cpx is available from Dick et. al. 2010. The sample was run as a 1400°C total fusion analysis initially, although when discovered that samples were not completely degassing at 1400°C the sample was re-run as a step heated experiment. The 1400°C total fusion analysis is not reported due to an assumed incomplete extraction of He.

JAS113-20**Lithology:** Oxide Gabbro**Location:** 23.471N, 45.359W. Cain Dome**Analysis:** Helium, Microprobe, LA-ICPMS

Image of JAS113-20 (right):

Red core is of the cpx (core is purely cpx)

Blue core is of the WR matrix (no cpx).

Black rectangle represents location of the thin section.

Comments: This sample proved to be degassed when run as a crushed analysis and 1400°C Total fusion analysis. This sample may be re-run as a step heated analysis with a 1600°C step in the future. The blue core location represents the site of both crushed and melted analysis. The cpx core was never melted.



JAS113-59b(3)

Lithology: Gabbro-norite vein in harzburgite

Location: 23.471N, 45.359W. Cain Dome

Analysis: Helium, LA-ICPMS

Image of JAS113-59b (right):

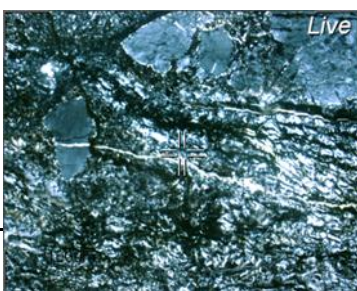
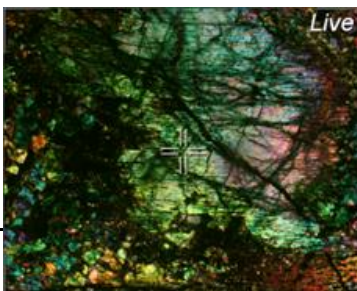
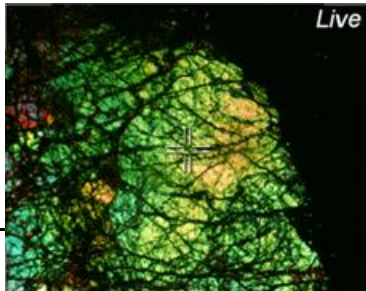
Red circle represent core of sample JAS113-59b(3)a* which was baked overnight at 100°C.

Blue dashed rectangle shows the location of where chips were taken for the melting and non-baked He analysis.

Black rectangle shows the location of one of the two thin sections taken of JAS113-59b.

Comments: The gabbro-norite vein runs through this complex sample which also contains serpentized (assumably) dunite veins cross-cutting a mylonitic harzburgite. The top of the rock contains a talco-gauge zone which is interpreted to represent the fault contact where the sample was exhumed. The gabbro-norite is serpentized and shows a large degree of heterogeneity.



Sample		JAS 113-59b		
Rock Name		Harzburgite with norite and dunite veins		
Hand Sample Description:				
Contains multiple layers. An ultramylonite host with serpentized dunite veins, a gabbro norite vein, and a talc-gauge where the rock was in contact with a fault wall. See Dick, 2008 for a greater description of the rock. Heavily serpentized everywhere except only moderately serpentized in the norite vein.				
Microscopic Description				
Vol%	Mineral	Size (mm)	Shape	Distinguishing Features
25	Orthopyroxene	<6mm	rounded	some bent laminae, may be from deformation
75	Serpentized olivine/black stuff	<1um		clear myloninzation patterns.
	<u>GABBRO</u>	<u>NORITE:</u>		
45	Clinopyroxene	<5mm	anhedral	Some are large with smaller cpx and olivine in cracks
40	Olivine	<4mm	anhedral	Not to bad looking, possible fluid inclusions.
15	Plagioclase	<3mm	anhedral	Altering, just one single large grain in thin section
Textual Features, Alteration, Deformation Grade, ect				
*Grade 3 mylonite by Kurz, 2009's standards. The harzburgite section can be classified as a mylonite, but little can be made of its mineralogy. The gabbro section cross cuts everything and is the freshest section, representing the last melt impregnation through the rock. The gabbro has course olivine and pyroxene which may account for the variability seen in each WR measurement. Olivines may have fluid inclusions or it might just be sample preparation blemishes. The talco-gauge section has hints of blueish hue representing either talc or chlorite.				
<div><div></div><div></div><div></div></div>				
Whole Rock	Mylonite	CPX (norite)	Olivine (norite)	
Field of View:	11mm	11mm	11mm	

KNR180-2 21-12:**Lithology:** Serpentine troctolite**Location:** 23.364N, 45.377W. Eve Dome**Analysis:** Helium


Image of KNR180-2 21-12 (right):

Red circle = All analysis comes from a large core.

Black rectangle = Approximate location of thin section.

Comments: This heavily serpentinized troctolite was interpreted in Dick et. al. (2010) as “olivine-rich troctolite interpreted as disaggregated dunite (Fo_{84.9}) impregnated by plagioclase (An_{66-72.9}) and granular clinopyroxene (Mg-number 87.6).” Thin section analysis by the author shows very little plagioclase, most of which is relicts from alteration. The olivines contains inclusions of spinel and fluid. The fluid inclusions occur as parallel lines of dark bubbles and were not samples during crushing analysis.



Sample		KNR 180-2, 21-12		
Rock Name		Troctolite		
Hand Sample Description:				
Pure black matrix with bits of white minerals and some cpx				
Microscopic Description				
Vol%	Mineral	Size (mm)	Shape	Distinguishing Features
~20	Clinopyroxene	<2.5	subhedral	extinction at ~60 to the 010 plane.
30	Olivine	<5	anhedral	"Torn" up veins of serpentine surrounds all the samples
40	Serpentine			Occurs as veins
10	opaques			White in hand sample, black opaque in thin section
Textual Features, Alteration, Deformation Grade, ect				
<p>Olivine does have clean shards between veins of serpentine, similar to Jas 112-84. Olivine contains small (<5um) fluid inclusions. Clinopyroxene contains no noticeable fluid inclusions. The white spots on the hand sample appear opaque in thin section. Some olivines contain square-ish spinel inclusions which appear almost glassy in transmitted light.</p>				
Photos:				
<p>Whole Rock Field of View 11mm</p>				

JAS 117-61:**Lithology:** Troctolite**Location:** 22.367N, 45.415W. Adam

Dome

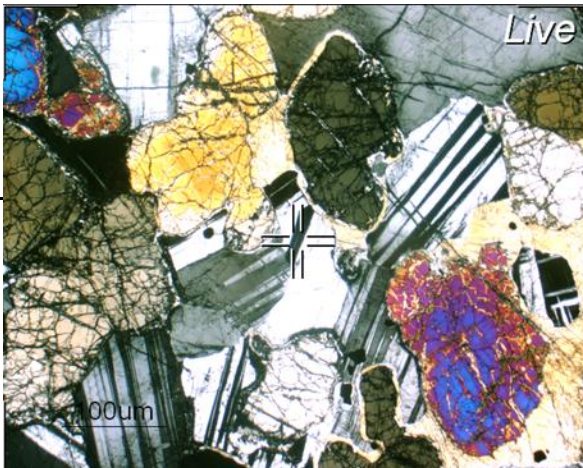
Analysis: Helium

Red circle= Large core which was run during two separate crushing analysis and melting.

Black Rectangle = Rough location of the thin section.

**Comments:** A very fresh troctolite with clinopyroxene representing trapped interstitial melt.

There are clean olivines with fluid inclusions throughout as well as spinel inclusions. For a very detailed analysis of this sample see Lissenburg and Dick (2008).

Sample		Jas 117-61		
Rock Name		Troctolite		
Hand Sample Description:				
Blotches of black (olivine) and grey (plagioclase), homogenously distributed at roughly cotectic proportions.				
Microscopic Description				
Vol%	Mineral	Size (mm)	Shape	Distinguishing Features
65	Olivine	2.0 -5.0	subhedral	Course fractured olivine pattern
25	Plagioclase	2.0 - 5.0	subhedral	Clean with albite twinning.
10	Clinopyroxene	0.1 - 0.8	unique	Found as an oikocryst with olivine and plagioclase in the chadacryst phase.
Textual Features, Alteration, Deformation Grade, ect				
A relatively clean troctolite with ~5-10% serpentatization of the olivines. CPX forms as a oikocryst around olivine and plagioclase. It is most commonly seen as thin ~100um rims around the individual crystals but it can be found as course as 800um incorporating both olivine and plagioclase. Lissenburg and Dick, 2008 interprets the data (combined with microprobe data) as a late stage melt impregnation into the troctolite host, which got trapped and crystalized.				
Photos:				
Field of View				
Whole Rock Image				
11mm				

JAS 117-62:

Lithology: Troctolite host with
diffusive gabbro vein

Location: 22.367N, 45.415W. Adam
Dome

Analysis: Helium, LA-ICPMS

Image of JAS117-62 (right):

Red circles = Gabbro samples
crushed, melted.

Blue circle= initial crushed sample contain both gabbro vein and troctolite host

Green circle= Troctolite host, ran as crushed and melted.



Comments: This sample occurs in two phases, a troctolite (~70% Olivine, 30% plagioclase) host and a gabbro vein composed of clinopyroxene and plagioclase. The gabbro vein is degassed while the troctolite contains some remnant of He away from the vein. Both phases are very fresh and contain fluid inclusions. Thin section analysis shows that there is little interaction between the two phases and olivine only occurs in the troctolite.

JAS 117-63:

Lithology: Troctolite Host with a
diffusive gabbro vein

Location: 22.367N, 45.415W. Adam
Dome

Analysis: Helium

Image of JAS117-63 (right):

Red Circle: Core of gabbro section, both
crushed and attempted melt

Blue Circle: Core of troctolite section both crushed and attempted melt

Green Circle: Initial crush incorporating both gabbro and troctolite.



Comments: Sample was initially run as a mixed core of gabbro and troctolite, then separate cores of pure troctolite and gabbro were analyzed (all degassed beyond detectability). Both the gabbro section and troctolite section were unsuccessfully melted after a malfunction in the furnace. It is more difficult to obtain a pure troctolite core in this sample due to the high amount of gabbro dispersed in all orientations. The polished face of the sample was cut-off before analysis to preserve the structure for any future research. See Lissenburg and Dick (2008) for more details on this sample and type 2 cpx.

KNR180-2 25-1:**Lithology:** Troctolite**Location:** 23.395N, 45.415W.

Adam Dome

Analysis: Helium

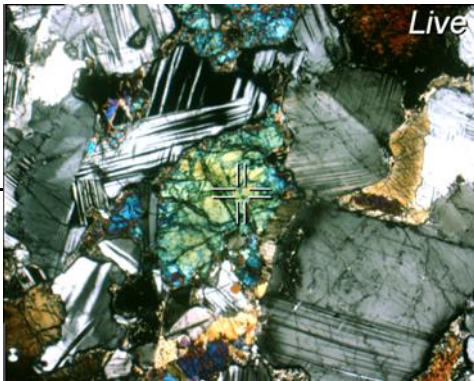
Image of KNR180-2 25-1 (right):

Red circle represents the core of
both crushing and melt analysis



Black rectangle represents approximate location of thin section. Sample was sawed in half (along face shown in image) in order to preserve structure prior to He sampling.

Comments: Minus the brown alterations along the edges this is a very fresh sample. Contained large olivines with fluids inclusions although less clinopyroxene than JAS 117-63. See Lissenburg and Dick (2008) for more details on this sample and type 1 cpx.

Sample		KNR 180-2 25-1		
Rock Name		Troctolite		
Hand Sample Description:				
Fresh				
Microscopic Description				
Vol%	Mineral	Size (mm)	Shape	Distinguishing Features
60	Plagioclase	<7mm	sub-euhedral	
30	Olivine	<5mm	Sub-euhedral	
10	Clinopyroxene	up to 500um		Found between and rimming olivine and plagioclase
Textual Features, Alteration, Deformation Grade, ect				
Near-cotectic composition troctolite with cpx forming around both plagioclase and olivines. Lissenburg and Dick, 2008 interpret this as trapped interstitial melt. Not many cpx rims in this sample, like seen in JAS117-61				
Photos:				
Whole Rock Field of View 11mm				

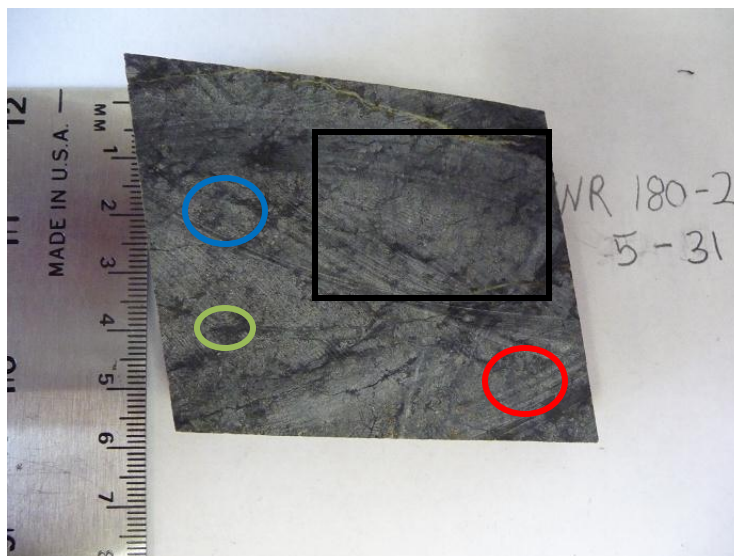
KNR180-2 5-31:**Lithology:** Olivine Websterite**Location:** 23.471N, 45.358W. Cain Dome**Analysis:** Helium, Microprobe, LA-ICPMS

Red circle: Location of crushed core sample and some mineral separates.

Blue circle: opx and cpx mineral separates.

Green Circle: Core for 1400°C total fusion and failed step heating analysis.

Black rectangle: Thin section location.



Comments: A fresh olivine websterite, the olivine in thin section contains small fluid inclusions and appears as a vein running through a matrix of clinopyroxene and orthopyroxene. The sample has a heterogeneous distribution of He which has been further complicated by the lack of step heating analysis for the whole rock and melting analysis for cpx. The hot blank prior to the 1400°C total fusion analysis contained very little He and thus the $^3\text{He}/^4\text{He}$ ratio of 8.6 R_A is believable, but the [He] is considered a minimum.

JAS112-64:**Lithology:** Orthopyroxenite**Location:** 23.477N, 45.350W. Cain
Dome**Analysis:** Helium

Image of JAS112-64 (right):

Red Circle: Core taken and used for
both crushing and total fusion
analysis.**Comments:** A disappointing sample, no thin sections were made of this sample so the cause for lack of He is currently unknown. The sample was only melted at 1400°C and may potentially release measureable He at a 1600°C step.

KNR180-2 28-34:**Lithology:** Harzburgite**Location:** 23.383N, 45.382W. Adam
Dome**Analysis:** Helium, Microprobe, LA-
ICPMS

Image of KNR180-2 28-34 (right):
opx and cpx separates were taken
from chunks of the rocks.



Comments: A heavily oxidized sample consisting of clean grains of clinopyroxene and orthopyroxene in a matrix of orangey-powder. The separates were quite fresh and clean after ultrasonicing them. Microprobe analysis was done on the grains which didn't crush to a fine powder (~15% of the sample) and confirmed the mineralogy. A few grains which were prepared for total fusion analysis were separated and analyzed using the LA-ICPMS for trace elements.

JAS112-84:**Lithology:** Porphyroclastic

Harzburgite

Location: 23.477N, 45.350W.

Cain Dome

Analysis: Helium, Microprobe,

LA-ICPMS

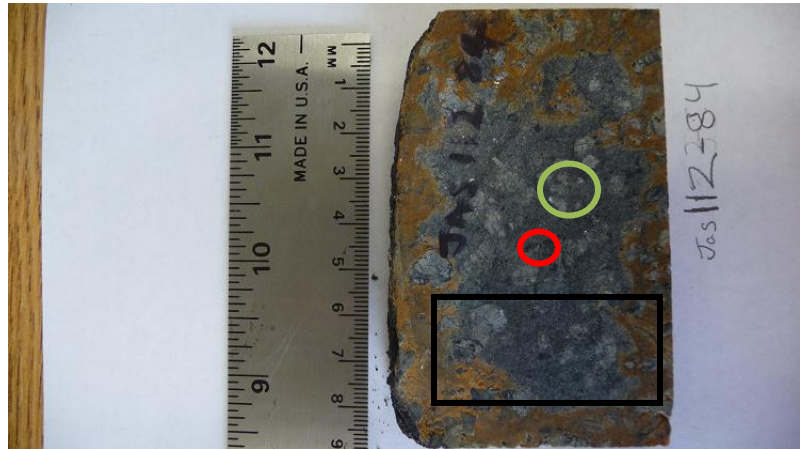


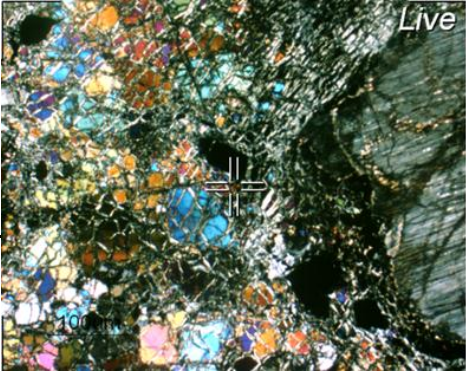
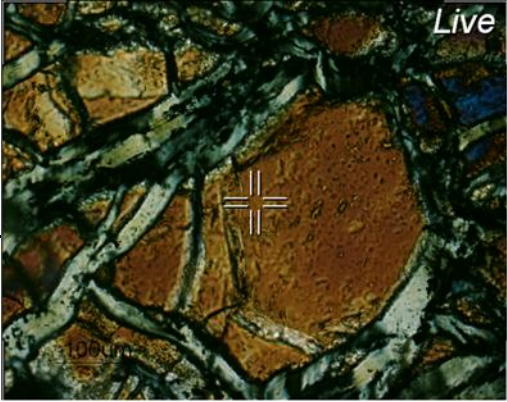
Image of JAS112-84 (right):

Red circle: The initial crushed core sample (baked overnight).

Green circle: The second core consisting of the second crushed sample and both total fusion and step heating experiments.

Black Rectangle: Location of the thin section.

Comments: The core of this sample is quite fresh, rims of serpentine surround each olivine grain but the grains are very clean and contain fluid inclusions. There are large orthopyroxene grains throughout the sample and some smaller clinopyroxene grains. The total fusion analysis at 1400°C for this sample revealed that 1400°C is not hot enough to melt a core of rock.

Sample	JAS 112-84			
Rock Name	Harzburgite			
Hand Sample Description:				
A relatively fresh harzburgite with porphyroclastic CPX crystals in a black olivine matrix. The rock sample contains an oxidized rim which is not seen in the core of the sample. By Kurz (2010) scale it is a grade 1 harzburgite.				
Microscopic Description				
Vol%	Mineral	Size (mm)	Shape	Distinguishing Features
60	Olivine	0.1 - 0.5	Euhedral - Subhedral	Appear to be ~250um olivine grains which are broken into clean shards by veins.
38	Orthopyroxene	1.0 - 5.0	Subhedral	Course crystals can be up to 5mm in diameter. Contain thin veins of serpentine.
2	other	< 0.25		Alteration, possibly some cpx and plagioclase mixed in there as well.
Textual Features, Alteration, Deformation Grade, ect				
Grade 1 porphyroclastic harzburgite. Opx are course with a few veins of serpentine running through them. Olivines are broken into small clean shards within each crystal by grayish veins (see picture below). Olivines appear to have 1-3um fluid/melt inclusions. Areas of oxidation show the same structure as fresh areas but are coated in a brownish color (black under cross polarized light). There is at least one instance of smaller (~250um) opx crystals surrounding a courser grain opx crystal. Olivine shows evidence for recrystallization from the smaller grain sizes surrounding the opx crystals.				
				
Whole Rock Field of View 11mm		Olivine 5.5mm		

JAS113-35:

Lithology: Harzburgite

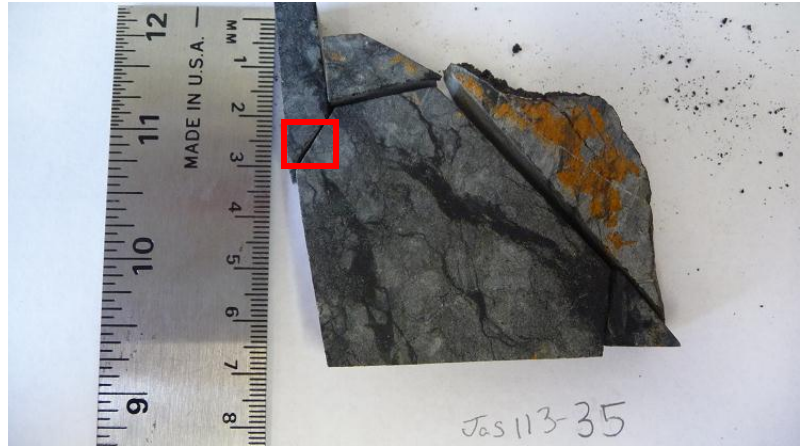
Location: 23.471N, 45.359W. Cain

Dome

Analysis: Helium

Image of JAS113-35 (right):

Red square: Location of chips taken
for WR analysis and opx separate.



Comments: Rock and opx separate contained no measureable gas when crushed. The sample was never melted due to issues with the furnace.

JAS112-49:

Lithology: Mylonitized

Harzburgite

Location: 23.477N, 45.350W. Cain

Dome

Analysis: Helium

Image of JAS112-49 (right):

Red Circle: Location of the core for
both crushing and melting analysis.



Comments: A mylonitic harzburgite, grade 2 with elongated coarse opx crystals. No thin section analysis was made of this sample.

JAS113-59a:

Lithology: Mylonitic harzburgite

Location: 23.471N, 45.359W. Cain
Dome

Analysis: Helium

Image of JAS113-59a (right):

Red Circle: Core for both crushed
and melted experiments.



Comments: A mylonitic plagioclase harzburgite, grade 3 with some opx and plagioclase crystals in a matrix of deformed serpentinite. Same rock as JAS113-59b(1).

KNR180-2 12-5:**Lithology:** Hydrous altered

harzburgite

Location: 23.607N, 45.286W. Cain

Dome

Analysis: Helium

Image of KNR180-2 12-5 (right):

Red Circle: Location of Crushed
analysis.

Comments: A very hydrously altered harzburgite. Contained high concentrations of H_2O and H_3 when crushed and thusly was not considered for melting experiments. Sample broke into multiple pieces after being drilled.

KNR180-2 17-18:

Lithology: Spinel Harzburgite

Mylonite

Location: 23.480N, 45.384W. Abel

Dome.

Analysis: Helium


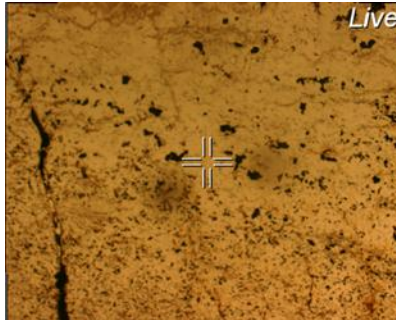
Image of KNR180-2 17-18 (right):

Representative WR cores were taken

but their location was not recorded.



Comments: A mylonite, grade 3 with clusters of spinel running along shear zones. Thin sections were taken of the sample for further analysis (below).

Sample		KNR 180-2, 17-18		
Rock Name		Spinel Harzburgite		
Hand Sample Description:				
Relatively fresh mylonite with dark patches of fine grain spinel crystals.				
Microscopic Description				
Vol%	Mineral	Size (mm)	Shape	Distinguishing Features
15	OrthroPyroxene	5	rounded	Only one large crystal in the thin section
80	Fine grained cpx olv, and alterations	up to 100um	anhedral	
5	spinel	100um & 10um	round-blocky	Two populations of spinel. Unsure of what each of them are, may be the same chemistry
Textual Features, Alteration, Deformation Grade, ect				
Grade goes from 3-4 depending on where you are in the sample. Spinels seem to be distributed in two populations, couser (100um) spinels are in different areas than the fine (10um) spinels. The finer spinels are clumped closer together and are more numerous.				
				
Whole Rock	11mm FOV	Whole Rock	transmitted light	11mm FOV

Basalt Glass:

AII 96 18-1: Good glass quality with minor vitrified rims. Some persistent oxide weathering products remained after physical scrapping and ultra-sonic cleaning. Vesicle size ~5% of surface area. No phenocrysts.

AII 96 18-2: Decent glass quality with spherulites pervasive throughout. Nearly all surface oxidation was removed prior to analysis. Vesicle size ~5% of surface. No phenocrysts.

G104 25-2: Decent glass quality with minor (~2 %) spherulites. Contained ~15% pervasive surface oxidation after cleaning. Vesicle size ~10% of surface area. No phenocrysts.

G104 25-3: Good quality glass with 10% spherulites. ~10% surface oxidation. Contained a thin crypto-crystalline rim. ~2 % plagioclase concentration.

G104 17-13: Good quality glass but only contained low volume platy sheets. Glass was well cleaned prior to analysis. No phenocrysts.

G104 2-1: Decent quality glass but only contained low volume platy sheets. Some slight filming on the surface of the glass. ~15 plagioclase concentration.

G104 20-21: Very good quality glass. No oxidation or phenocrysts. Contains a 'Bubbly' surface morphology.

AII 96 8-2: Good quality glass with similar ‘Bubbly’ surface texture as G104 20-21. Contained small amounts of oxidation prior to analysis.

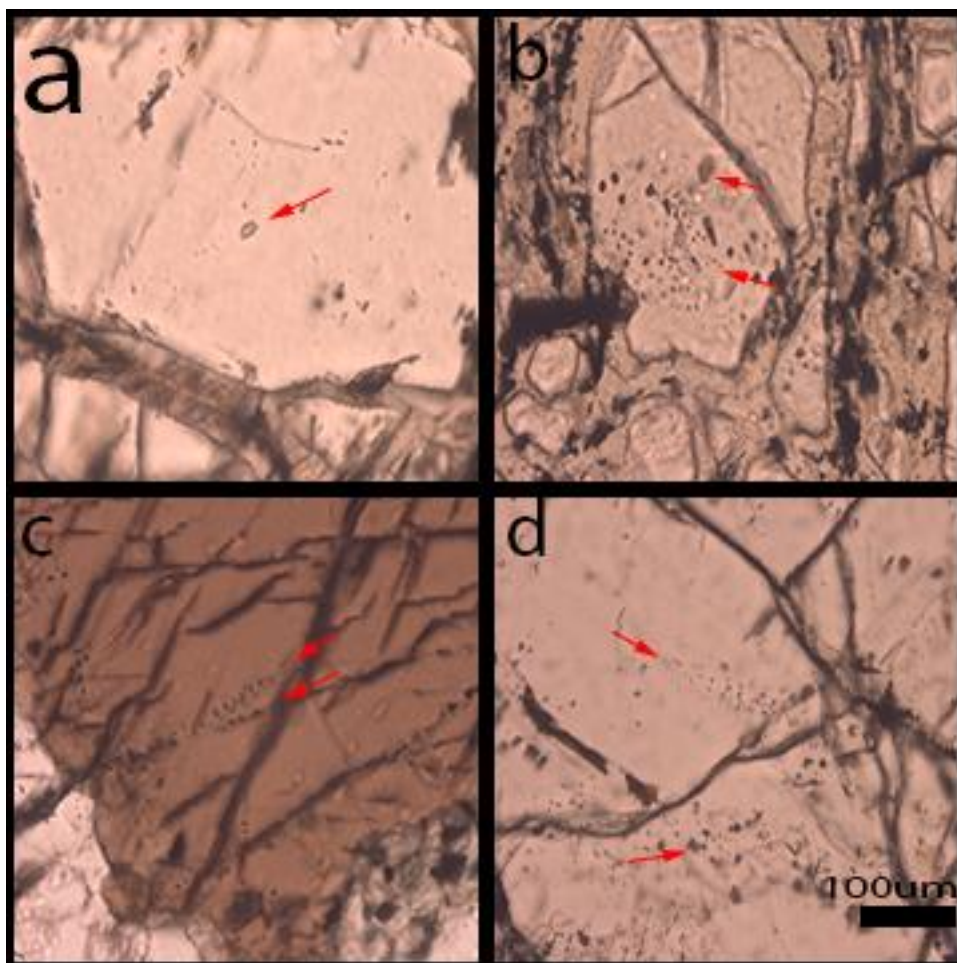


Figure A1: Images of inclusions (fluid and melt) using a petrographic microscope under transmitted light at 40x zoom. Arrows point to the location of inclusions. The scale bar for all images is 100 μm . A.) KNR180-2 21-12, a clean olivine shard containing a melt inclusion. B.) JAS112-84, a harzburgite showing clean olivine with numerous bands of both fluid and melt inclusions. C.) KNR180-2 5-30, a mylonitized gabbro containing amphibole with bands of fluid inclusions running through the z-axis. D.) KNR180-2 25-1, a troctolite showing large planes of fluid inclusions in olivine.